

# On resonances in open systems

By STEFAN HEIN<sup>1</sup>, THORSTEN HOHAGE<sup>2</sup>  
AND WERNER KOCH<sup>1</sup>

<sup>1</sup>Institut für Aerodynamik und Strömungstechnik, DLR Göttingen, Germany

<sup>2</sup>Institut für Numerische und Angewandte Mathematik, Universität Göttingen, Germany

(Received 18 August 2003 and in revised form 22 December 2003)

An open system or open resonator is a domain of wave activity separated from the exterior by a partly open or partly transparent surface. Such open resonators lose energy to infinity through radiation. The numerical computation of the corresponding resonances is complicated by spurious reflections of the outgoing waves at the necessarily finite grid boundaries. These reflections can be reduced to extremely low levels by applying perfectly matched layer (PML) absorbing boundary conditions, which separate the discrete resonances from the continuous spectrum. Using a simple one-dimensional model problem, the influence of the various PML parameters is determined by a numerical error analysis. In addition to one-dimensional open resonators, two-dimensional open resonators as well as various resonating structures in waveguides are considered, and the resonant spectra and selected modes are evaluated. For the first time, leaky modes are computed for several resonating structures in a waveguide in addition to the trapped modes published in the literature. In applications, leaky mode resonances are often more important than trapped mode resonances. Gap tones, observed in a model problem of high-lift configurations, are identified as transversal resonant modes with the lowest radiation losses.

---

## 1. Introduction

Resonances are of importance in many wave propagation problems with bounding surfaces. Usually they manifest themselves by a large response of the system to external excitation. If the surface separating an interior from an exterior domain is partly open or partly transparent, we speak of an open system or open resonator. The main difference between open and closed resonators is that in the absence of dissipative losses the resonant frequencies of closed resonators are real, whereas those of open resonators are typically complex owing to radiation losses. For open resonators this results in a reduced modal density, i.e. often only a few modes have a quality factor high enough to be of physical significance. Energy is radiated away from the open resonator via so-called leaky waves. Instead of Dirichlet or Neumann boundary conditions, a radiation condition, allowing only outgoing waves, has to be imposed.

A typical and well-known example of an open acoustic resonator is a violin with two types of resonances, namely wood resonances and air resonances (Hutchins 1962). Here we are only interested in air resonances. According to Hutchins, a pioneer in violin acoustics, the frequency of the main air resonance (together with the wood resonance) is an important indicator of the quality of a violin. The vibrations inside the violin are communicated to the outside through the f-holes in the top of the instrument. The resonant air frequencies of the violin are then determined by the air

volume of the instrument body together with the form and area of these f-holes. As far as we know only approximate boundary conditions have been used at the f-holes for the computation of resonances in such a complicated geometry, cf. Elejabarrietta, Santamaria & Ezcurra (2002). However, an ever increasing number of computational aeroacoustics (CAA) publications shows the growing need for predicting acoustic resonances more exactly for complex open geometries.

Massive research efforts have been directed towards the exploration of electromagnetic resonances in open resonators because they play an important role as oscillatory systems in numerous applications such as lasers, light-emitting diodes, channel drop filters, etc. It is not surprising that Bérenger (1994) applied his perfectly matched layer (PML) technique first to electromagnetic waves. In most cases, this PML method has been used for time-domain problems, but typical examples for frequency-domain resonance computations of electromagnetic waves are Hyun *et al.* (1997) and Hwang *et al.* (1998). Applying the analytical Wiener–Hopf technique and the approximate parabolic method, the classical monograph by Weinstein (1969) is one of the few treating resonances in open systems. An extensive literature exists also for gravitational waves in the open systems of astrophysics where the resonant modes are usually termed quasi-normal modes, see for example Kokkotas & Schmidt (1999) and the literature cited therein. However, we are not aware of any application of the PML technique in this field, contrary to elastic waves where PMLs have been used in the problem of locating buried land mines (Schröder & Scott 2000).

Resonances can also have detrimental effects by causing large forces or sound pressure levels. Maniar & Newman (1997) and Evans & Porter (1997) demonstrated impressively how the hydrodynamic load of resonant water waves impinging on a long but finite single or double array of bottom-mounted cylinders in a finite-depth ocean can reach a multiple of that experienced by a single cylinder. This has obvious consequences for offshore and harbour engineering. Resonances might even be the reason for extraordinary high tsunami waves in an archipelago. The acoustic Parker modes, cf. Parker (1966) or the review by Parker & Stoneman (1989), are related to the above water wave resonances, and are well known for causing high sound pressure levels in compressor blade rows or pipe bundles of heat exchangers. Such acoustic resonances can also cause instabilities in aircraft engines (Cooper & Peake 2000; Vahdati *et al.* 2002), potentially leading to a greater susceptibility to fan blade flutter and/or rotating stall.

The numerical computation of resonances in open systems is complicated by the reflection of the leaky waves at the necessarily finite-grid boundaries. The PML method of Bérenger (1994) allows a reduction of these leaky wave reflections to extremely low values, and quickly became the method of choice also for other wave propagation problems (Hu 2004). In the present paper, PML absorbing boundary conditions are used to compute resonances numerically in open systems, mainly for acoustic waves. Near such resonances, transients linger for many periods before radiating out of the structure. This leads to a dramatic increase in time needed for time-domain computations before the time-harmonic steady state is obtained. To reach a deeper understanding of resonances in open resonators, and for a better feeling for their direct numerical computation via PMLs, we introduce various model problems of increasing complexity. At least some of these model problems are amenable to analytic solution and allow a comparison with our computational results. The present investigation is intended to prepare the ground for the computation of resonances in high lift devices where slat noise, together with the noise from flaps and landing gears, is one of the major sources of airframe noise (Grosche, Schneider & Stiewitt 1997;

Khorrami, Berkman & Choudhari 2000; Dobrzynski, Gehlhar & Buchholz 2001; or Olson 2003 and the literature cited therein).

## 2. Perfectly matched layer absorbing boundary conditions

In order to model open system wave propagation problems numerically, the computational domain is usually truncated and non-reflecting, transparent or absorbing boundary conditions (ABC) are employed to avoid or reduce non-physical reflections of outgoing waves at the finite-grid boundaries. Such reflections at the numerical boundaries are often the source of significant errors in the numerical computation, and a sizeable literature exists in this very active research area, cf. the reviews by Ihlenburg (1998), Tam (1998), Tsynkov (1998), Turkel & Yefet (1998), Givoli (1999) or Hu (2004). The PML technique proposed by Bérenger (1994) for the finite-difference time-domain solution of electromagnetic wave propagation problems provided a breakthrough in performance and quickly became the method of choice in the computational electromagnetics community. Using a split-field formulation, Bérenger enlarged the computational domain by artificial absorbing layers. The main difference to other absorbing layer methods is that Bérenger constructed his PML equations in such a way that the PML interface is theoretically reflectionless for outgoing electromagnetic waves at any frequency and angle of incidence. When implemented in discrete form, the matching is not perfect, but the results are still significantly more accurate than those obtained with most other ABC.

Within a short time, alternative formulations of the PML method were proposed using unsplit physical variables, cf. the anisotropic PML of Sacks *et al.* (1995), or the complex coordinate stretching method of Chew & Weedon (1994), Chew, Jin & Michielssen (1997). The PML method was extended to the frequency domain and was also applied successfully in other fields, such as elastic wave propagation (Hastings, Schneider & Broschat 1996; Schröder & Scott 2000), or computational aeroacoustics (Hu 1996; Tam, Auriault & Cambuli 1998). For the linearized Euler equations, numerical instabilities of earlier PML formulations were eliminated by Hu (2001, 2002), providing perfectly matched boundary conditions also for vorticity and entropy waves.

The complex coordinate stretching PML formulation is strikingly similar to complex scaling methods in the theory of quantum resonances. There the Aguilar–Balslev–Combes–Simon theory (Aguilar & Combes 1971; Baslev & Combes 1971; Simon 1973) provides a powerful tool for the numerical computation of resonances in atomic and molecular physics, as discussed in the monograph by Hislop & Sigal (1996), or reviewed by Moiseyev (1998). It is somehow surprising that despite the similarities there appears to be no cross-referencing between these two communities. In a closed-region problem resonances are the real eigenvalues of a self-adjoint operator. In an open-region problem resonances are either complex or real and embedded in the continuous spectrum. In the case of real resonances, we speak of trapped modes. Non-trapped resonance eigenfunctions grow exponentially in space, and consequently are no longer in the  $L^2$  Hilbert space. According to the Aguilar–Balslev–Combes–Simon theory, resonances can be defined and numerically computed as the eigenvalues of a spectrally deformed operator, and the eigenfunctions of this spectrally deformed operator are square integrable.

In acoustics, the propagation of small disturbances in a medium with zero mean flow is governed by the wave equation. The propagation velocity  $c^*$  is the speed of sound. Here, and in the following, the star superscript marks dimensional quantities. We formulate our problems in two-dimensional Cartesian coordinates  $(x^*, y^*)$  which

are non-dimensionalized with a characteristic reference length  $l_{ref}^*$ . Furthermore, all velocities are non-dimensionalized with a reference wave speed  $c_{ref}^*$ , densities with  $\rho_{ref}^*$  and pressures with  $\rho_{ref}^* c_{ref}^{*2}$ . The particular reference quantities will be listed for each individual example. Assuming harmonic time dependence  $\exp(-i\omega^* t^*)$ , where  $\omega^*$  is the circular frequency, the wave equation reduces to the non-dimensional Helmholtz equation,

$$\Delta\phi + (K/c)^2\phi = 0, \quad (2.1)$$

for the velocity potential  $\phi(x, y)$ . Here,  $K = \omega^* l_{ref}^*/c_{ref}^*$  is a non-dimensional frequency, the so-called Helmholtz number. The time-independent dimensionless disturbance velocity and pressure are then given by  $\mathbf{v}(x, y) = \nabla\phi$  and  $p(x, y) = iK\rho\phi$ , respectively.

For two-dimensional Cartesian coordinates, the PML method works as follows: in the PML domain we continue  $\phi(x, y)$  analytically with respect to the variables  $(x, y) \in \mathbb{R}^2$  to the complex variables  $(\xi, \eta) \in \mathbb{C}^2$ . The extended solution  $\tilde{\phi}(\xi, \eta)$  satisfies the same differential equation as  $\phi$ :

$$\frac{\partial^2 \tilde{\phi}}{\partial \xi^2}(\xi, \eta) + \frac{\partial^2 \tilde{\phi}}{\partial \eta^2}(\xi, \eta) + (K/c)^2 \tilde{\phi}(\xi, \eta) = 0. \quad (2.2)$$

Now we choose some paths

$$\xi(x) = x + i\sigma_x(x), \quad \eta(y) = y + i\sigma_y(y). \quad (2.3)$$

The spatial variation of the damping functions  $\sigma_x(x)$  and  $\sigma_y(y)$  is usually chosen in power form, smoothly starting at the PML interface at  $x = \pm x_0$  in the  $x$ -direction, or  $y = \pm y_0$  in the  $y$ -direction, e.g.

$$\sigma_x(x) = \begin{cases} \sigma_{x,0} (x - x_0)^\beta, & x > x_0, \\ 0, & |x| \leq x_0, \\ -\sigma_{x,0} (-x - x_0)^\beta, & x < -x_0, \end{cases} \quad (2.4)$$

$$\sigma_y(y) = \begin{cases} \sigma_{y,0} (y - y_0)^\beta, & y > y_0, \\ 0, & |y| \leq y_0, \\ -\sigma_{y,0} (-y - y_0)^\beta, & y < -y_0, \end{cases} \quad (2.5)$$

with damping coefficients  $\sigma_{x,0}, \sigma_{y,0}$  and a shape parameter  $\beta \geq 1$ . For comparison, we show some of the complex scalings used in the theory of quantum resonances in figure 1. The above scalings (2.4) and (2.5) correspond to the ordinary exterior scaling in figure 1.

By the chain rule, the function  $\phi_{PML}(x, y) := \tilde{\phi}(\xi(x), \eta(y))$  satisfies the elliptic differential equation

$$\frac{1}{\xi'(x)} \frac{\partial}{\partial x} \left( \frac{1}{\xi'(x)} \frac{\partial \phi_{PML}}{\partial x} \right) + \frac{1}{\eta'(y)} \frac{\partial}{\partial y} \left( \frac{1}{\eta'(y)} \frac{\partial \phi_{PML}}{\partial y} \right) + (K/c)^2 \phi_{PML} = 0, \quad (2.6)$$

which involves an anisotropic damping tensor, compare also Turkel & Yefet (1998). It can be seen that  $\phi$  is outgoing if and only if  $\phi_{PML}(x, y)$  decays exponentially as  $|x| \rightarrow \infty$  and  $|y| \rightarrow \infty$ . This suggests imposing homogeneous Dirichlet conditions at some finite distances  $\pm(x_0 + d_x)$  and  $\pm(y_0 + d_y)$ :

$$\phi_{PML}(\pm(x_0 + d_x), y) = 0, \quad \phi_{PML}(x, \pm(y_0 + d_y)) = 0. \quad (2.7)$$

Here  $d_x$  and  $d_y$  are the widths of the PML in the  $x$ - and  $y$ -directions respectively, and we arrive at a finite domain eigenvalue problem, which can be solved numerically by standard codes.

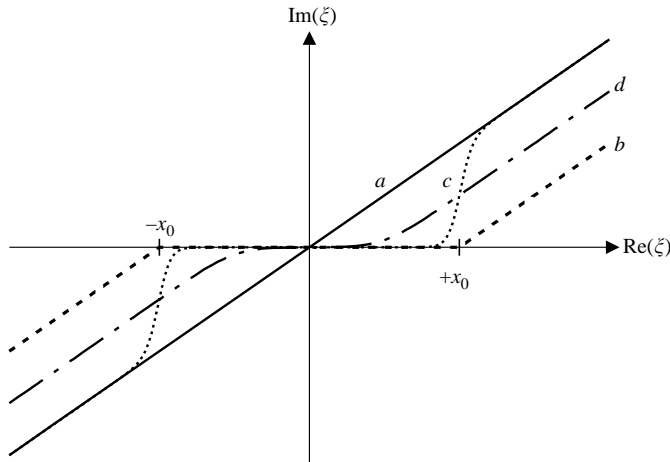


FIGURE 1. Complex scalings used in the theory of quantum resonances (cf. Karlsson 1998): (a) ordinary complex scaling, (b) ordinary exterior scaling, (c) smooth exterior scaling (Taylor form), (d) smooth exterior scaling (Woods–Saxon form).

### 3. Resonances in one-dimensional open systems

Before we proceed with the computation of resonances in two-dimensional open systems, it is helpful to study resonances in one-dimensional model systems. One of the simplest models is the acoustic resonances in a plane layer of finite thickness  $l^*$  with uniform  $\rho_1^*, c_1^*$  embedded in an infinite medium with  $\rho_0^*, c_0^*$ . This problem is amenable to analytical solution and gives us the rare opportunity to quantify the influence of the various PML parameters by comparing our numerical solution with the exact analytical result.

#### 3.1. Acoustic resonances in a plane layer

The problem of acoustic resonances in a plane layer of finite-thickness  $l^*$ , as sketched in figure 2(a), is closely related to the text book example of normal wave reflection and transmission, cf. Brekhovskikh (1960) or Pierce (1981).  $l^*, \rho_1^*$  and  $c_1^*$  are chosen as reference quantities. For one-dimensional acoustic disturbances in a medium with  $c = c_j$ , equation (2.1) reduces to

$$\frac{d^2\phi}{dx^2} + (K/c_j)^2\phi = 0. \tag{3.1}$$

Here,  $K = \omega^* l^* / c_1^*$ , and the time-independent dimensionless disturbance velocity in the  $x$ -direction and the disturbance pressure are given by  $u(x) = d\phi/dx$  and  $p(x) = iK\rho_j\phi$ , respectively. Then the solution of (3.1) for the problem depicted in figure 2 can be expressed in the form

$$\phi(x) = \begin{cases} E_0 \exp(i(K/c_0)x) + R_0 \exp(-i(K/c_0)x), & x \leq -1/2, \\ A_1 \exp(iKx) + B_1 \exp(-iKx), & -1/2 < x < +1/2, \\ T_0 \exp(i(K/c_0)x), & x \geq +1/2. \end{cases}$$

Matching velocity and pressure at the interfaces  $x = \pm 1/2$ , results in a system of four equations for the four unknown wave amplitudes  $R_0, A_1, B_1$  and  $T_0$ , with the incoming wave amplitude  $E_0$  prescribed. The solution of this system of algebraic

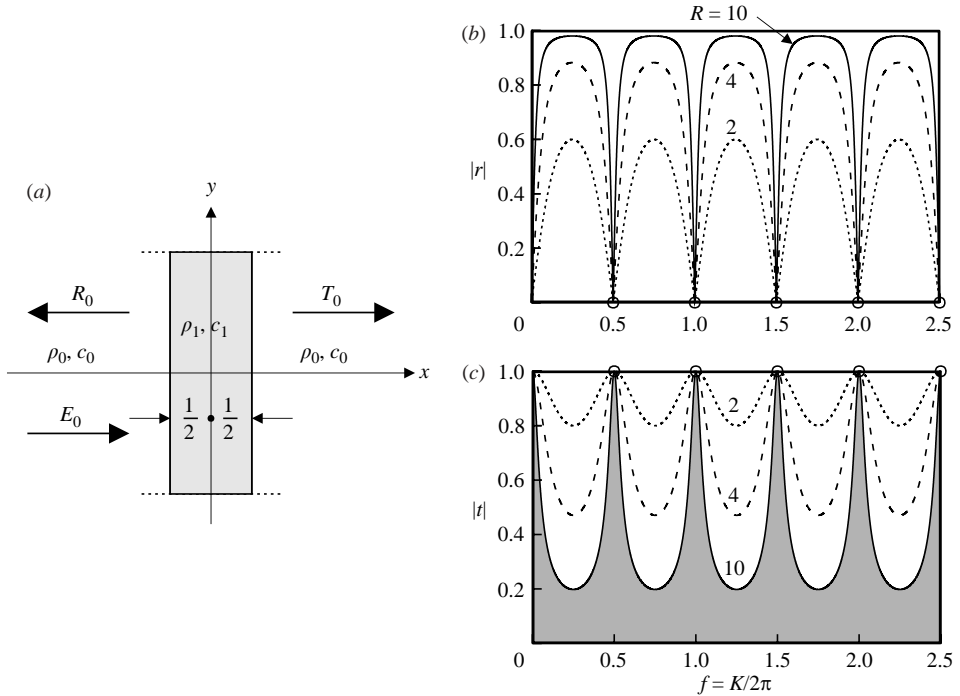


FIGURE 2. Wave reflection and transmission from a plane layer: modulus of amplitude reflection factor  $|r|$  and amplitude transmission factor  $|t|$  as function of frequency  $f$  and impedance parameter  $R$ .

equations gives the well-known amplitude reflection factor  $r$  (up to a phase shift)

$$r = \frac{R_0}{E_0} = \frac{-i[R - R^{-1}] \sin K}{2 \cos K - i[R + R^{-1}] \sin K}, \quad (3.2)$$

derived for example in Brekhovskikh (1960) or Pierce (1981). Figure 2 depicts the modulus of the amplitude reflection and transmission factor (defined as the ratio of amplitude of the reflected or transmitted wave to the amplitude of the incoming wave) as a function of the non-dimensional (real) frequency  $f = K/(2\pi)$ . The abbreviation  $R = (\rho_1 c_1)/(\rho_0 c_0)$  denotes the ratio of the characteristic impedances.

For  $E_0 = 0$ , a non-vanishing solution  $\phi$  exists only if the determinant of the above-discussed system of algebraic equations vanishes. This corresponds to finding the roots of the denominator of (3.2), i.e.

$$K = K_n = n\pi - i \ln((R + 1)/(R - 1)) \quad n = 1, 2, \dots \quad (3.3)$$

The (complex) frequencies  $f_n = f_{n,r} + i f_{n,i} = K_n/(2\pi)$  are termed natural or resonant frequencies of the finite-thickness layer, and the corresponding functions  $\phi_n(x)$  are called free, resonant, or quasi-normal modes. The real part of the resonant frequencies  $f_n$ , marked by circles in figure 2, coincides exactly with the zeros of  $|r|$ , corresponding to  $|t| = 1$ , i.e. where perfect transmission occurs. The imaginary part is the same for all resonances and is always less than zero as a consequence of radiation losses. The quality factor

$$Q = \left| \frac{f_r}{2f_i} \right|, \quad (3.4)$$

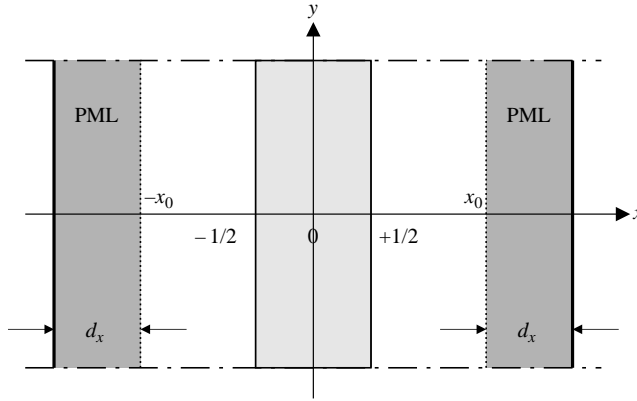


FIGURE 3. Single layer with perfectly matched layers located at  $\pm x_0$ .

is a measure for the resonator’s ability to store energy. From (3.3), we see that  $Q$  increases with  $n$ .

Now that we have an analytical solution, we solve the same problem numerically by placing perfectly matched layers of thickness  $d_x$  at  $x = \pm x_0$  as sketched in figure 3. The solution is either symmetric or antisymmetric about  $x = 0$ . Therefore, we need to solve only for  $x \geq 0$  with the boundary condition  $\phi(0) = 0$  for antisymmetric, or  $d\phi/dx(0) = 0$  for symmetric resonances. For the numerical discretization, we used a multi-domain Chebyshev spectral collocation method in the  $x$ -direction, cf. Canuto *et al.* (1988), with  $N_{x,col}$  collocation points in each domain. In the PML, equation (2.6) reduces to

$$\frac{d^2\phi_{PML}}{dx^2} - \frac{\xi''(x)}{\xi'(x)} \frac{d\phi_{PML}}{dx} + (\xi'(x)K/c_j)^2\phi_{PML} = 0. \tag{3.5}$$

Essentially, this is a Helmholtz equation with a complex wavenumber and a damping term if  $\xi''(x) \neq 0$ . At the end of the PML, we impose the Dirichlet boundary condition  $\phi_{PML}(x_0 + d_x) = 0$ . At the interface  $x = x_0$  between the PML and the regular domain, the matching conditions are now  $d\phi/dx = (d\phi_{PML}/dx)/\xi'$  and  $\rho\phi = \rho_{PML}\phi_{PML}$ , i.e. the velocity is discontinuous if  $\xi' \neq 1$  at  $x = x_0$ .

After discretization, a generalized algebraic eigenvalue problem is obtained, which can be solved by standard global eigenvalue solvers. Figure 4 shows a comparison of the numerical spectrum with the analytical resonant frequencies (3.3). Owing to the PML, the continuous spectrum is shifted towards the negative imaginary axis and is clearly separated from the physically relevant resonances. The circles depict the analytical resonances (3.3) which coincide quite well with the numerically computed resonances. Also shown is a comparison of the numerical and analytical eigenfunction of two resonant modes, corresponding to the two resonances marked by the solid dots in the eigenvalue spectrum. We can see that the numerical solution is strongly damped in the PML, and behaves like a standing wave within and like a travelling wave outside the plane layer. The figure also demonstrates that the resonant modes are damped in time but diverge exponentially in space, which in the past caused mathematical as well as conceptual problems with regard to their physical meaning.

With the analytical solution (3.3) given explicitly, we can compute the relative error as a function of the various PML parameters, as shown in figure 5 for the fundamental eigenvalue  $n = 0$ . For the iterative computation of a single eigenvalue we used the local Wieland iteration, cf. Zurmühl (1961, p. 289ff). We distinguish between

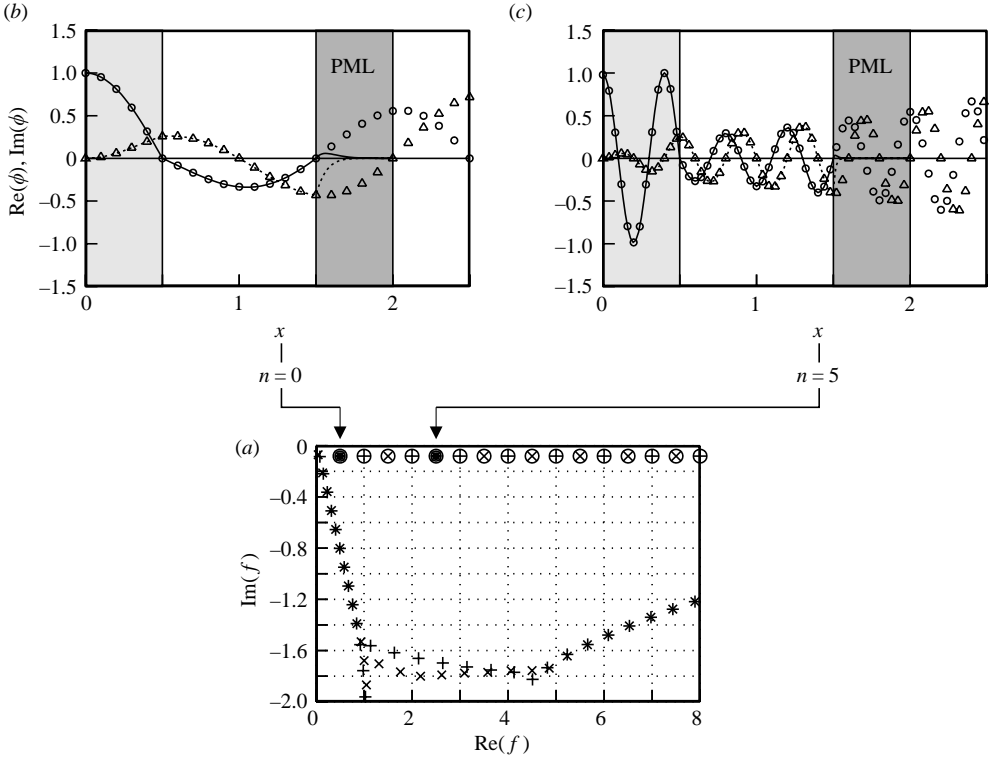


FIGURE 4. Single-layer resonance: (a) spectrum of symmetric ( $\times$ ) and antisymmetric ( $+$ ) numerical eigenvalues together with the analytical resonances (3.3) marked by ( $\circ$ ).  $R=4$ ,  $N_{x,col}=45$ ,  $\sigma_{x,0}=5$ ,  $x_0=1.5$ ,  $d_x=0.5$ ,  $\beta=1$ . (b) and (c) show the real (solid line) and imaginary (dashed line) part of the first (b) and third (c) symmetric eigenfunction corresponding to the eigenvalues marked by the solid dots in the spectrum. The real and imaginary parts of the analytical eigenfunction are depicted by the symbols  $\circ$  and  $\Delta$ , respectively.

the numerical discretization error in  $|x| \leq x_0$ , and the error due to the finite thickness and discretization in the PML. The numerical discretization error can be obtained by imposing Dirichlet boundary conditions at  $x = \pm 0.5$ , and is shown in all parts of figure 5 by the line with solid circles. It can be seen that the relative error with PMLs is always larger than the numerical discretization error as a consequence of the numerical implementation of the finite-thickness PML. Therefore, increasing the number of domains outside the PML does not improve the accuracy. However, the accuracy can be improved considerably by increasing the number of domains within the PML (or equivalently the number of points in the PML), as demonstrated by the examples marked by solid symbols in figures 5(a) and 5(b). Around  $10^{-12}$  rounding errors limit the accuracy. Aside from the well-known trends that the accuracy can be improved by either increasing the damping coefficient  $\sigma_{x,0}$  or the PML thickness  $d_x$ , see for example Qi & Geers (1998), we make the following observations:

(i) For given PML parameters and before reaching the rounding error limit, the error curve levels off owing to reflections at the end of the PML and cannot be improved by higher discretization. Quantitatively, this level is fixed by the value of the damping function  $\sigma_x(x_0 + d_x)$  at the end of the PML.



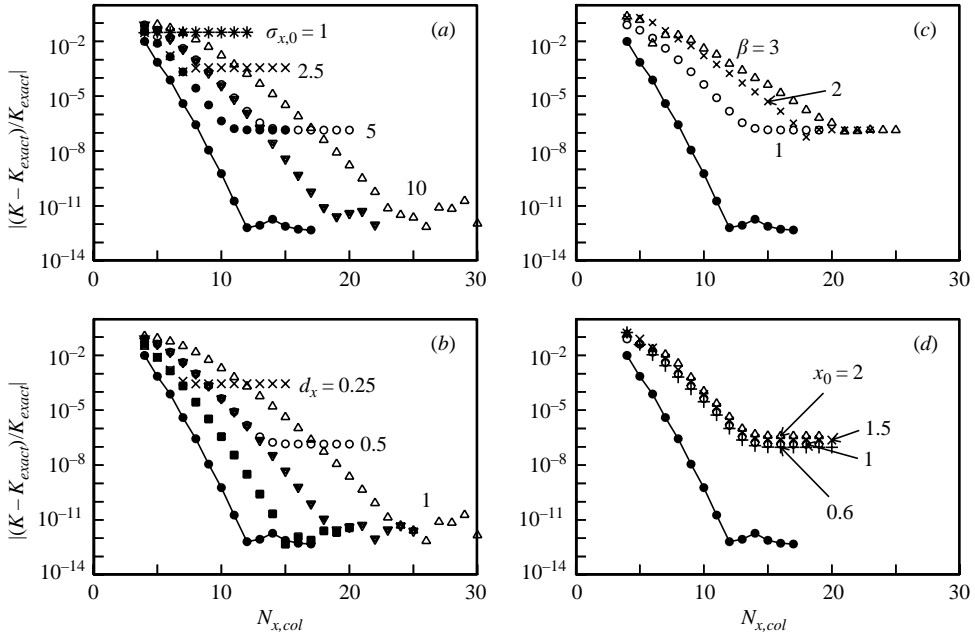


FIGURE 5. Single-layer resonance: relative error of fundamental eigenvalue  $n=0$  as a function of  $N_{x,col}$  and various PML parameters. (a) Variation of damping coefficient  $\sigma_{x,0}$  with  $d_x=0.5, \beta=1, x_0=1$ . (b) Variation of PML thickness  $d_x$  with  $\sigma_{x,0}=5, \beta=1, x_0=1$ . (c) Variation of shape parameter  $\beta$  with  $\sigma_{x,0}=5, d_x=0.5, x_0=1$ . (d) Variation of distance  $x_0$  with  $\sigma_{x,0}=5, \beta=1, d_x=0.5$ . The line with solid circles in all plots gives the numerical discretization error for the closed resonator with Dirichlet boundary conditions prescribed at  $x=0.5$ . The filled circles and triangles in (a) and (b) represent the error after halving the PML domain  $d_x=1$  and keeping the same number of collocation points in each half, i.e. doubling the points in the PML. The filled squares in (b) result if the first half of the PML is halved again, resulting in three PML domains with the same number of collocation points in each domain.

(ii)  $\beta = 1$  gives the highest accuracy before reaching this levelling off, cf. figure 5(c). This is surprising because most PML computations use a parabolic variation of the damping function  $\sigma_x(x)$ . In all our computations we use  $\beta = 1$ .

(iii) The error seems rather insensitive to the distance of the PML from the resonating layer, cf. figure 5(d). The slightly higher error for larger  $x_0$  is probably due to the slightly higher amplitude of the exponentially increasing outgoing wave at larger  $x_0$ .

In summary, using the analytical solution of the simple model problem, a numerical error analysis has been performed demonstrating the influence of the various PML parameters and providing a guide for their choice.

### 3.2. Fabry–Perot resonator

The one-dimensional acoustic resonator model for a single layer discussed above is so simple that it is hard to believe that it has not been used before for PML parameter studies. At least we are not aware of any such investigation. On the other hand, we found a related and only slightly more complicated example in optics, namely the Fabry–Perot resonator. The Fabry–Perot resonator consists of two parallel imperfect mirrors separated by a cavity of width  $t_C$ , cf. Fowles (1968) or Meyer & Pottel (1969). In order to obtain a high value of reflectance (for example in lasers) each mirror is

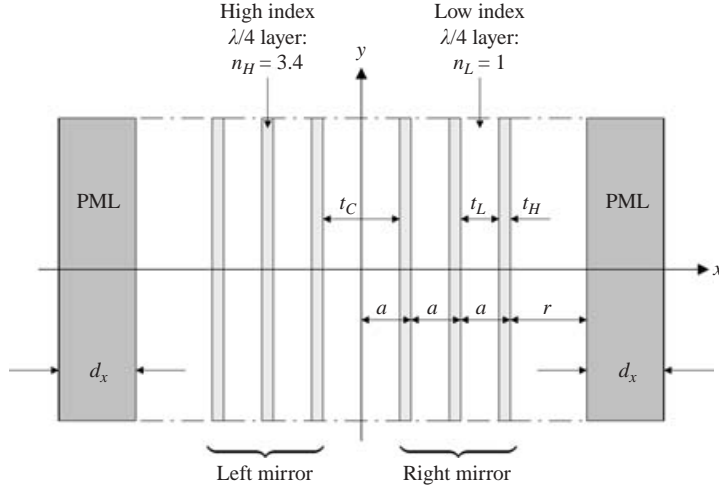


FIGURE 6. Fabry–Perot resonator with perfectly matched layers, cf. Hyun *et al.* (1997).

made up of a stack of alternate layers of high refractive index,  $n_H$ , and low refractive index,  $n_L$ , materials, the thickness of each layer being  $1/4$  wavelength. Here the index of refraction  $n$  is defined as the ratio of the speed of light in vacuum  $c_\infty^*$  to its speed in the medium, and we use  $c_{ref}^* = c_\infty^*$  as reference wave speed in this example.

Using the finite-element method and the anisotropic PML boundary condition, Hyun *et al.* (1997)<sup>†</sup> investigated such a Fabry–Perot resonator, see figure 6, as a one-dimensional model for a truncated photonic crystal. We shall use the example of Hyun *et al.* (1997), in which the high-index layer has a refractive index  $n_H = 3.4$  and a thickness  $t_H = a/(n_H + 1)$ . The low-index layer has a thickness  $t_L = an_H/(n_H + 1)$  and a low refractive index  $n_L = 1$  (air). The central cavity has a width  $t_C = 2t_L$ . The scaling factor  $a$  denotes the thickness of a pair of layers, i.e.  $t_L + t_H = a$ , and, following Hyun *et al.* (1997), has been set equal to 1, i.e.  $a^*$  is now taken as reference length  $l_{ref}^*$ . The spacing  $r$  between the Fabry–Perot mirror and the PML is taken to be  $2t_L$ .

This electrodynamic problem is governed by Maxwell’s equations, but can be reduced to the Helmholtz equation, (3.1), if we substitute  $E_y$  for  $\phi$  and  $n_j$  for  $1/c_j$ . Here,  $E_y$  is the  $y$ -component of the electric field vector with all other components being zero. The Helmholtz number for the electrodynamic problem is now defined as  $K = \omega^* a^* / c_\infty^*$ . The only non-zero component of the magnetic field is  $H_z$  (transverse magnetic mode). At the interface between two media with different index of refraction  $n$ , the tangential components of the electric and magnetic field are continuous, i.e.  $E_y$  and  $H_z$  are continuous. For non-magnetic media, the continuity of  $H_z$  implies the continuity of  $dE_y/dx$ . With these interface conditions, the above described Fabry–Perot resonator problem can be solved analytically as well as numerically using PMLs, and constitutes a simple model for resonances in a multi-layer system.

Figure 7 shows the spectra and sample resonance functions for mirrors with one and three high-index layers. Here the reduced frequency  $f$  is defined by

$$f = \omega^* t_L^* / (c_\infty^* \pi) = K t_L / \pi. \quad (3.6)$$

The numerical spectra show again a clear separation of the resonances from the rotated discretized continuous spectrum near the imaginary axis. Hyun *et al.* (1997)

<sup>†</sup> We are grateful to Jeong-Ki Hwang for providing us with additional information.

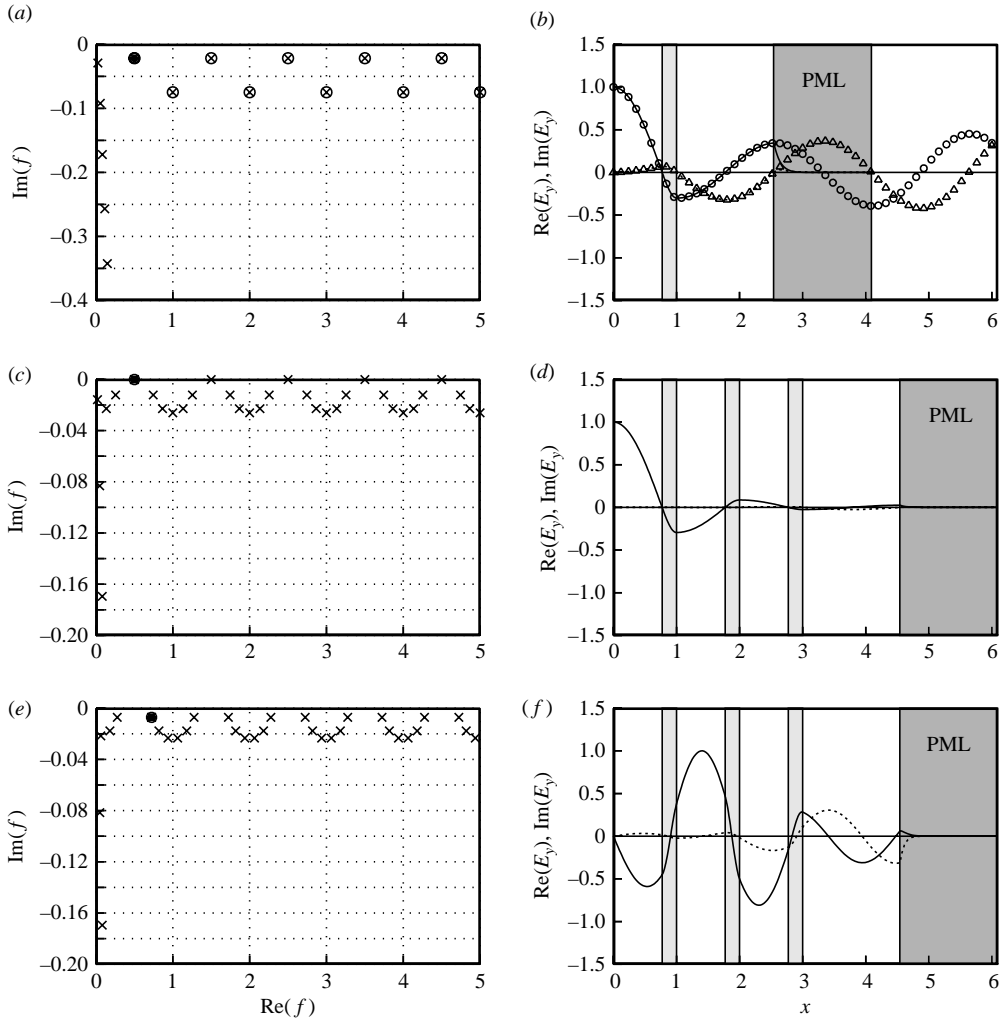


FIGURE 7. Fabry–Perot resonator: spectra and resonant functions for mirrors with one (a,b) and three (c–f) high-index layers.  $N_{x,col} = 45$ ,  $\sigma_{x,0} = 5$ ,  $\beta = 1$ ,  $r = d_x = 2t_L$ . (a) and (c) are the spectra for the symmetric eigenfunctions while (e) shows antisymmetric eigenvalues. The circles in (a) mark the analytical resonances for comparison. The real and imaginary parts of the analytical resonance  $E_y$  in (b), corresponding to the fundamental mode marked by the solid dot in (a), are again depicted by the symbols  $\circ$  and  $\triangle$ , respectively, while the numerical results are given by the solid and dashed curve, respectively. (d) shows the symmetric fundamental eigenfunction  $E_y$  corresponding to the mode marked by the solid dot in (c), while (f) shows the antisymmetric eigenfunction  $E_y$  belonging to the mode marked by the solid dot in (e).

solved the problem depicted in figure 7(d) where the mirrors consist of three high-index layers. We can see that with an increasing number of mirror layers, the number of resonances increases and the imaginary part of  $f$  decreases, implying lower radiation losses and higher reflectance.

For a better understanding of the various resonances, we varied the cavity length  $t_C$  and computed each eigenvalue iteratively via Wielandt iteration, starting with the case  $t_C = 2t_L$  of Hyun *et al.* (1997). The corresponding results for the symmetric resonant

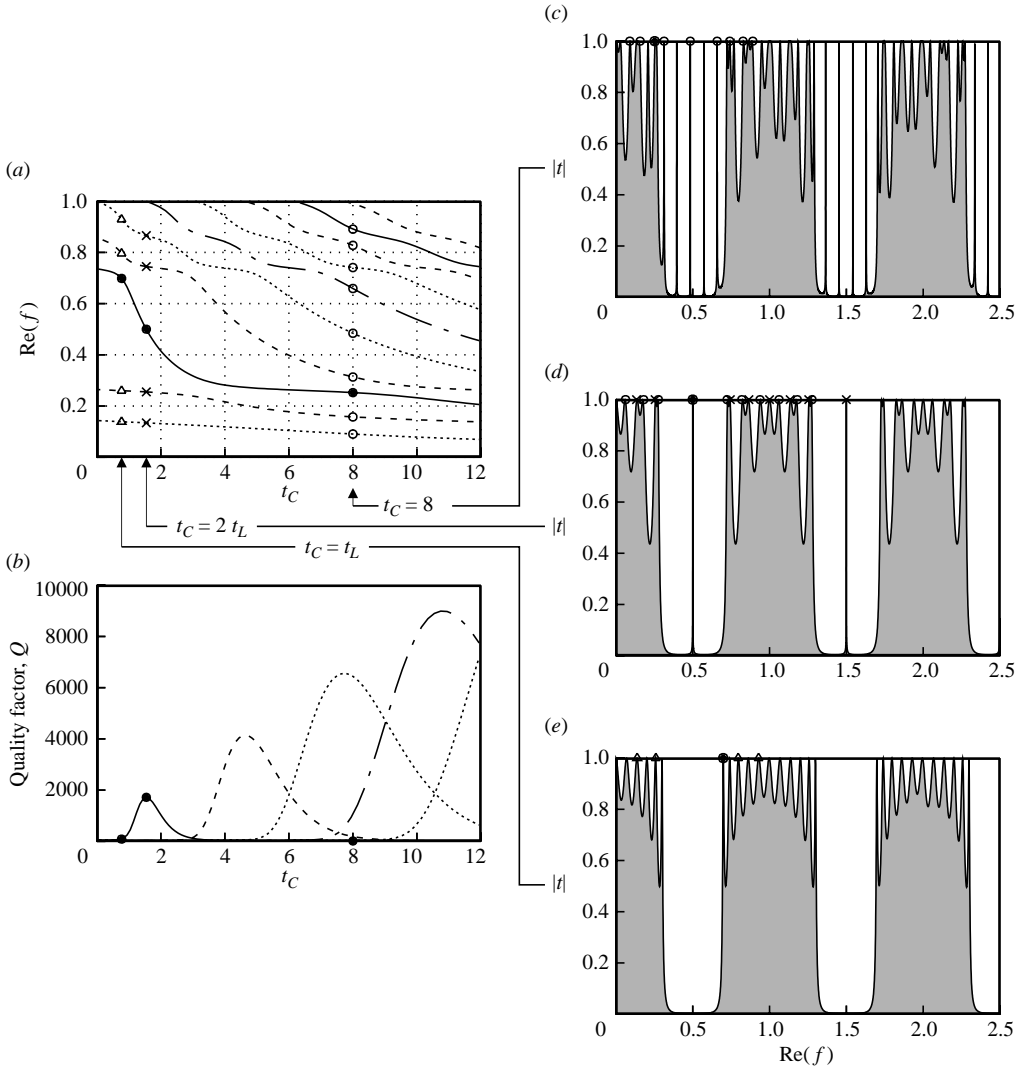


FIGURE 8. Fabry–Pérot resonator: (a) variation of resonant frequencies with cavity length  $t_C$  and (b) corresponding  $Q$  factor. Modulus of amplitude transmission factor  $|t|$  for (e)  $t_C = t_L$ , (d)  $t_C = 2t_L$ , and (c)  $t_C = 8$ .

frequencies  $0 < \text{Re}(f) < 1$  of figure 7(c) are reshown in figure 8(a,b). We see that only the mode marked by the solid dot in figure 7(c), and at  $t_C = 2t_L$  in figure 8(a), gives a higher  $Q$  factor. If  $t_C$  is increased, higher resonant modes show maxima of the  $Q$  factor at  $\text{Re}(f) = 0.5$ , and the  $Q$  factor is much higher than that for the fundamental mode. Similar results are obtained at  $\text{Re}(f) = 1.5$ , etc. To demonstrate the reason behind this behaviour, we computed the amplitude transmission factor for three different  $t_C$ , and depicted the modulus of the amplitude transmission factor  $|t|$  in figures 8(c), 8(d) and 8(e). We obtained these amplitude transmission (and reflection) factors simply by solving the system of interface conditions at the various interfaces between high- and low-index layers (transmission matrix approach).

Figure 8(e) shows the amplitude transmission factor for  $t_C = t_L$ , i.e. for exactly five periodic low-index layers between six high-index layers. This is essentially a truncated one-dimensional photonic crystal, and we observe stopbands with zero transmission around  $f = (n + 1)/2, n = 0, 1, \dots$  (such frequency regions are called photonic bandgaps analogous to electronic bandgaps in semiconductors), and passbands around  $f = n, n = 0, 1, \dots$ . The many peaks in the passbands of the transmission factor of figure 8(e) are exactly the resonant frequencies marked by triangles in figure 8(a) (the unmarked peaks in between are those from the antisymmetric resonances).

If we introduce a ‘defect’ into the photonic crystal by adding a cavity with  $t_C \neq t_L$ , the band structure essentially remains, but some of the resonant modes move into the stopband (so-called defect modes) with extremely sharp resonances corresponding to high  $Q$  factors. In figure 8(d) for  $t_C = 2t_L$ , the case treated by Hyun *et al.* (1997), we see that one resonance is exactly in the middle of the stopbands. The crosses (and the solid circle for the  $f = 0.5$  resonance) in figure 8(d) correspond exactly to the symmetric resonances up to  $\text{Re}(f) = 1.5$ , marked by crosses in figures 7(c) and 8(a). The open circles in figure 8(d) correspond to the antisymmetric resonances, marked by crosses and the solid circle in figure 7(e). Finally, in figure 8(c) for  $t_C = 8$ , several resonances moved into the stopband, and the symmetric resonances, marked by circles in figure 8(a), are also marked by circles in figure 8(c). Qualitatively similar results have been found for geometrically more complex two-dimensional Fabry–Perot structures using a boundary integral formulation or scattering matrix theory (Venakides, Haider & Papanicolaou 2000; Kriegsmann 2003). In these papers, the photonic crystal mirrors are built up by parallel columns of circular dielectric rods instead of the parallel dielectric layers of figure 6.

Summarizing, we can say that for multi-layer one-dimensional systems, more or less distinct bandgaps occur in the transmission factor, and of the many resonances only those in the bandgaps (the defect modes) have high  $Q$  factors and will be of physical interest.

#### 4. Resonances in two-dimensional laterally periodic open systems

By adding lateral periodicity to our one-dimensional model of § 3.1, a second length  $d^*$  is introduced in addition to  $l^*$ . Important examples of laterally periodic open resonators are structures in a waveguide, or periodic structures like blade cascades, diffraction gratings or antennas. Some sample rectangular structures in a waveguide are shown in figure 9.

For waveguide problems it is customary to choose  $l_{ref}^* = d^*$  as reference length. At higher frequencies, more than one duct mode is cut-on, i.e. propagating. This means that multi-modal scattering is possible for these problems, with more than one reflected and transmitted wave, contrary to the examples of § 3. All structures depicted in figure 9 display symmetries. This is not necessary, but simplifies the computation. Although these models are highly idealized, the general solution method might have direct application in the technology of sintering ceramic materials by means of microwave energy, see for example Hile & Kriegsmann (1998).

##### 4.1. Resonances in a laterally bounded layer

In this section, we concentrate on the model shown in figure 9(a). In the shaded layer, we prescribe a higher density  $\rho_1^*$  than in the surrounding fluid with  $\rho_0^*$ , but assume that the wave speed  $c_1^* = c_0^*$  is the same. This problem is amenable to straightforward

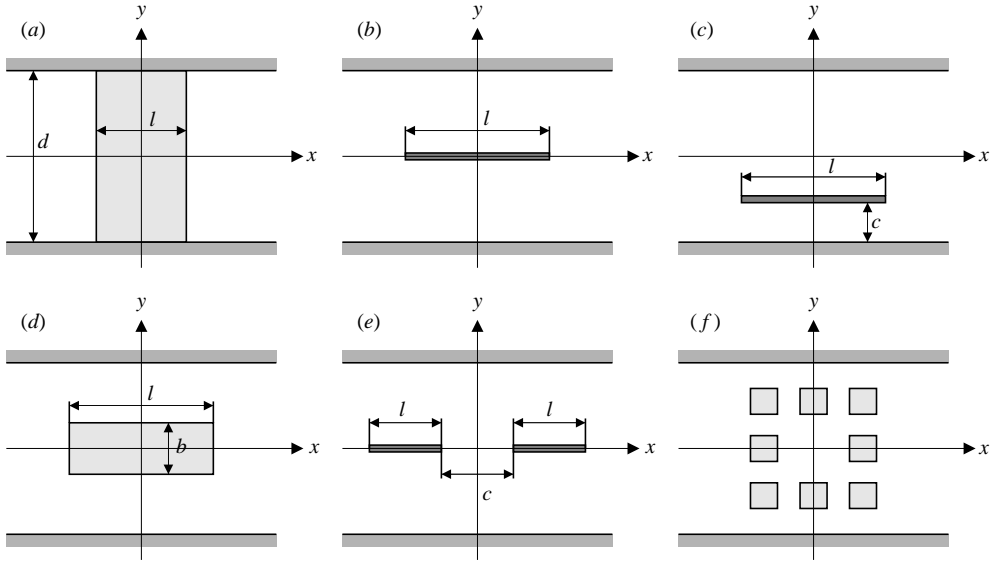


FIGURE 9. Various examples of rectangular structures in a waveguide. The shaded areas either mark materials with a different density and/or refraction index, or are solid bodies.

solution via separation of variables. The reference quantities are taken to be  $\rho_0^*$ ,  $c_0^*$  and  $d^*$ , such that  $K = \omega^* d^* / c_0^*$  and  $f = K / 2\pi$ . For sound-hard duct walls  $\partial\phi/\partial y(\pm 0.5) = 0$  we can split the solution into resonances symmetric and antisymmetric about the  $x$ -axis. The separation of variables solution of (2.1) for  $y$ -symmetric resonances with  $c = 1$  and  $d = 1$  is then of the form

$$\phi(x, y) = C^\pm \exp(\pm i\sqrt{K^2 - (2m\pi)^2}x) \cos(2m\pi y), \quad m = 0, 1, 2, \dots \quad (4.1)$$

Here the square root is defined uniquely by introducing a branch cut along the negative real axis and defining  $\sqrt{-x} = i\sqrt{x}$ ,  $x > 0$  on the branch cut. Matching  $x$  velocity and pressure across the interface, together with satisfying the radiation condition, we obtain the analytical  $y$ -symmetric resonances

$$K_{n,m} = \sqrt{(K_n/l)^2 + (2m\pi)^2}, \quad n = 1, 2, \dots, \quad m = 0, 1, 2, \dots, \quad (4.2)$$

where  $K_n$  is given by (3.3). Each resonant mode may be characterized by two integers  $(n, m)$  specifying the number of nodal lines of the pressure in the  $x$ - and  $y$ -directions, respectively. For  $l/d \equiv l = 2$  these analytical resonances are depicted in figure 10(a). For  $m = 0$  (and setting  $l = 1$  in (4.2) because we used  $l^*$  as reference length there) the one-dimensional resonances (3.3) are recovered. We observe that all two-dimensional resonances are less damped than the one-dimensional ones, and for fixed  $m \neq 0$  the resonances with  $n = 1$  are least damped.

For the numerical computation of the resonances we use a two-dimensional multi-domain Chebyshev collocation method with  $N_{x,col}$  and  $N_{y,col}$  collocation points in the  $x$ - and  $y$ -directions, respectively for each domain. The resonances can again be separated into resonances symmetric and antisymmetric about the  $y$ -axis, so that we have to solve only for  $x \geq 0, y \geq 0$ . A one-dimensional PML, starting at  $x_0$ , is sufficient to damp the outgoing waves, and the PML equation (2.6) reduces to

$$\frac{\partial^2 \phi_{PML}}{\partial^2 x^2} + \xi'^2(x) \frac{\partial^2 \phi_{PML}}{\partial^2 y^2} - \frac{\xi''(x)}{\xi'(x)} \frac{\partial \phi_{PML}}{\partial x} + (\xi'(x)K/c_j)^2 \phi_{PML} = 0. \quad (4.3)$$

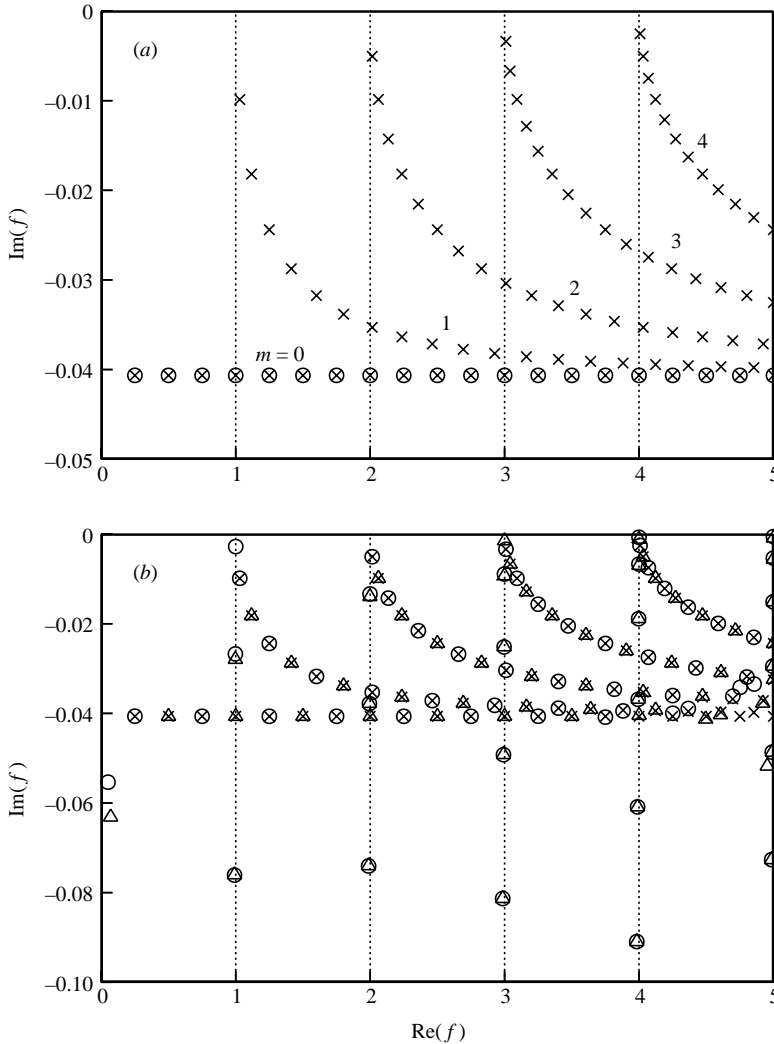


FIGURE 10. Single-layer  $y$ -symmetric resonances in a waveguide:  $\rho_1/\rho_0=4$  and  $l/d=2$ . (a) Analytical spectrum: the one-dimensional resonances  $m=0$  of figure 4 are marked by circles. (b) Comparison of analytical spectrum ( $\times$ ) with the  $y$ -symmetric  $x$ -symmetric ( $\circ$ ) or  $y$ -symmetric  $x$ -antisymmetric ( $\triangle$ ) numerical resonances:  $N_{x,col} = N_{y,col} = 30$ ,  $\sigma_{x,0} = 5$ ,  $x_0 = 2.5$ ,  $d_x = 0.5$ ,  $\beta = 1$ .

Figure 10(b) shows a comparison of the numerically obtained  $y$ -symmetric resonances with the corresponding analytical results (4.2). In addition to the numerical approximation of the continuous spectrum originating at  $f=0$  we now obtain a continuous spectrum for each symmetrical cut-on mode at  $\text{Re}(f)=1, 2, \dots$ . As can be seen, the numerical resonances agree quite well with the analytical results for low values ( $n, m$ ). Similar results are obtained for the  $y$ -antisymmetric resonances with cut-on frequencies at  $\text{Re}(f)=0.5, 1.5, \dots$

The analytical results (4.2) can again be used to compute the relative error. The results are qualitatively (and even quantitatively) close to the one-dimensional results of figure 5. We therefore suspect that the optimal PML depth found by Hyun *et al.* (1997), who used a periodic boundary condition in their two-dimensional finite-element

code in order to obtain the one-dimensional result, might be an artefact of their numerical solution. Some of the other structures depicted in figure 9 might be of interest for electromagnetic waves. However, in the following section we concentrate on acoustic problems, where the shaded structures in figure 9 are hard-walled bodies.

#### 4.2. Parker mode resonances

In many applications, wakes behind bodies, such as turbomachinery blades, guide vanes, supporting struts, etc., act as time-periodic sources which can excite resonances in open flow systems. Parker and his collaborators were the first to demonstrate that in many cases these resonances are of a purely acoustic nature and may lead to serious vibrations and/or unacceptably high noise levels (Parker 1966; Parker 1967), or the survey paper (Parker & Stoneman 1989). They showed that mechanical vibrations of the wake-shedding body play no direct role in these problems, i.e. the resonant frequencies and corresponding resonant modes depend only on the geometrical boundary of the open configuration, but are independent of the material properties of the wake-shedding body. Similar resonances were observed for water waves, cf. Maniar & Newman (1997) or Evans & Porter (1997), and quantum waveguides, see for example Exner *et al.* (1996). The publications by Ursell (1987) and Evans, Levitin & Vassiliev (1994) provide the mathematical background and cite relevant older literature.

Practically all publications up to now were only concerned with so-called *trapped* modes, also termed *bound states* in other fields. These are localized oscillations at discrete frequencies having finite energy. Trapped modes are closely related to the non-uniqueness of the forced-motion problem, and therefore attracted considerable attention, see for example Evans & Linton (1991) and Callan, Linton & Evans (1991). Neglecting dissipation, they persist for all time in the absence of external forcing, i.e. they are undamped and no energy is radiated to infinity. As a consequence, trapped modes decay towards infinity, which is the reason why the numerical computation of Parker (1967) on a finite-sized grid worked. Contrary to these trapped modes, resonant modes are damped due to radiation losses, and are therefore often termed *leaky* modes. Nevertheless, these leaky modes are at least equally important, as can be seen in figure 1(a) of Maniar & Newman (1997), where these leaky modes cause even higher loads than the trapped mode. Trapped modes are just very special resonant modes.

In the following, we start with the classical Parker-mode problem, i.e. a finite-length plate of length  $l$  and zero thickness placed symmetrically in a channel, cf. figure 9b. On the plate, the normal velocity has to vanish, i.e.  $\partial\phi/\partial y(x, 0) = 0$ ,  $-l/2 \leq x \leq +l/2$ . On the channel walls either Neumann boundary conditions  $\partial\phi/\partial y(x, \pm 0.5) = 0$  (Neumann problem) or Dirichlet boundary conditions  $\phi(x, \pm 0.5) = 0$  (Dirichlet problem) are applied. Contrary to the model problem of §4.1, no exact solution is known for the Parker-mode problem. However, several approximate solutions, obtained by various methods, have been published, such as Franklin (1972), who used a variational formulation, Nayfeh & Huddleston (1979) and Evans & Linton (1994), who applied the mode matching technique, or Koch (1983), Evans & Linton (1991) and Woodley & Peake (1999), who used the Wiener–Hopf method. The approximation usually consists of truncating an homogeneous infinite system of linear algebraic equations, and in many cases low truncations give very accurate results.

In our purely numerical approach, we apply the PML method as described in the previous section and take advantage of the symmetries. Figure 11 shows the spectrum



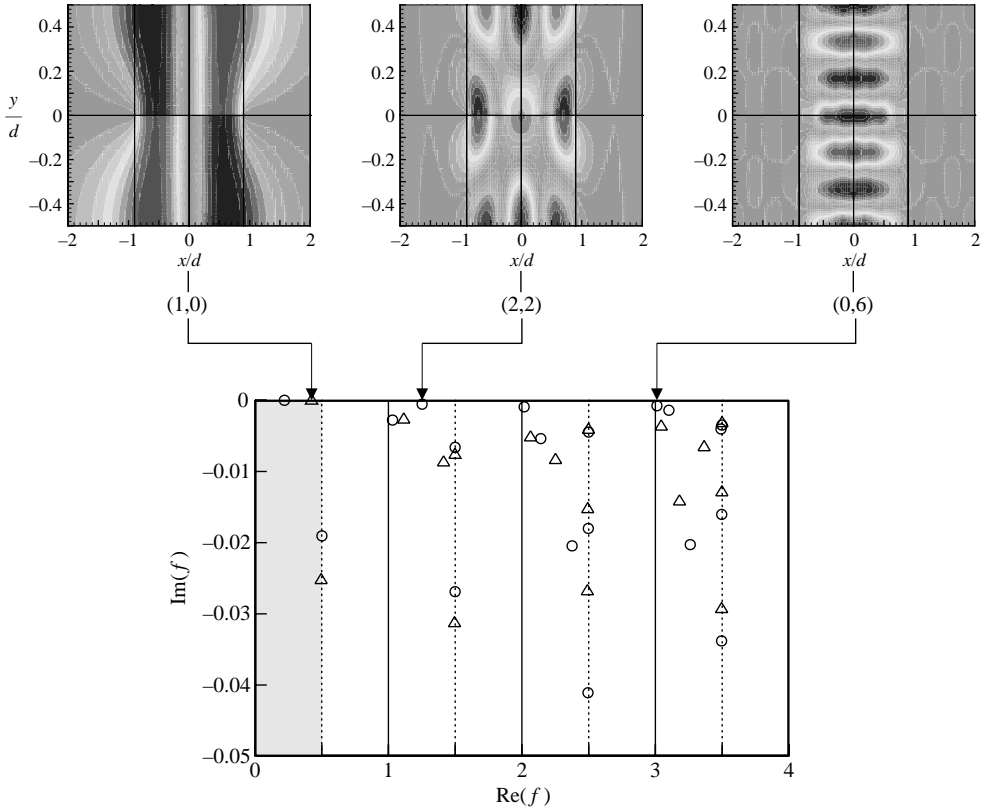


FIGURE 11. Parker mode resonances for the Neumann problem with  $l/d=1.8$ .  $N_{x,col} = N_{y,col} = 30$ ,  $\sigma_{x,0} = 5$ ,  $d_x = 0.5$ ,  $\beta = 1$ .  $\circ$ ,  $x$ -symmetric;  $\triangle$ ,  $x$ -antisymmetric resonances. The top pictures show three examples of resonant eigenfunctions  $\text{Re}(\phi)$ , computed with the higher resolution  $N_{x,col} = N_{y,col} = 40$  and the PML starting at  $x_0 = 2$ .

for the Neumann problem, where we separated the  $x$ -symmetric modes (marked by open circles) from the  $x$ -antisymmetric modes (marked by open triangles). The shaded area indicates the region of the hitherto treated trapped Neumann modes – in this example, Parker’s classical  $\alpha$  and  $\beta$  mode. In addition to the resonant modes, our numerical result also contains an approximation to the continuous spectra of the cut-on modes beginning at  $\text{Re}(f) = 0.5, 1.5, \dots$ . However, these can be separated fairly easily from the resonant modes in between. While the two trapped modes are (theoretically) undamped, we see that only a few weakly damped resonant modes exist, i.e. with  $\text{Im}(f) \ll 1$ . Only these weakly damped modes have a  $Q$  factor high enough to be of physical importance. In the top pictures of figure 11, three resonant eigenfunctions are depicted, including Parker’s  $\alpha$  mode  $(1, 0)$ . Again, all modes can be ordered by two integers  $(n, m)$  corresponding to the number of nodal lines in the  $x$ - and  $y$ -directions.

Similarly, figure 12 shows the corresponding spectrum for the Dirichlet problem. Now the continuous spectra start at  $\text{Re}(f) = 1, 2, \dots$ , and we distinguish again between  $x$ -symmetric (filled circles) and  $x$ -antisymmetric (filled triangles) modes. The shaded trapped-mode domain now contains three modes, including Parker’s  $\gamma$  and  $\delta$  mode. From figures 11 and 12, it appears that all higher-order weakly damped resonant modes are laser-like  $(0, m)$  transversal modes.

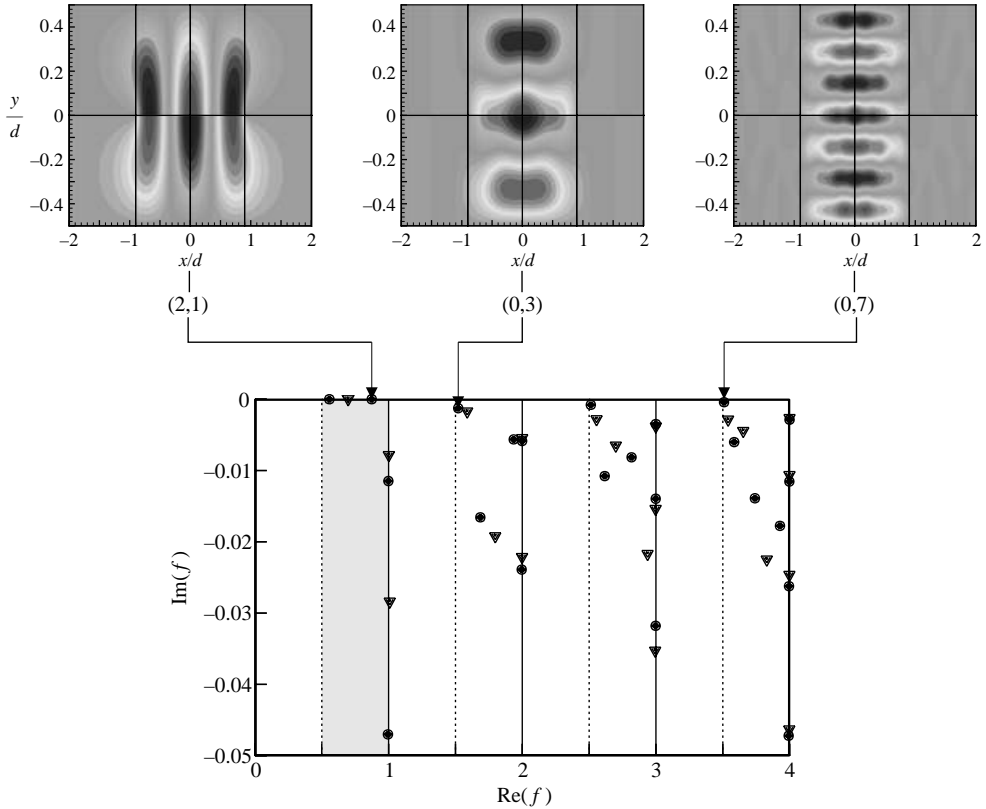


FIGURE 12. Parker mode resonances for the Dirichlet problem with  $l/d=1.8$ .  $N_{x,col} = N_{y,col} = 30$ ,  $\sigma_{x,0} = 5$ ,  $d_x = 0.5$ ,  $\beta = 1$ .  $\bullet$ ,  $x$ -symmetric;  $\blacktriangledown$ ,  $x$ -antisymmetric resonances. The top pictures show three examples of resonant eigenfunctions  $\text{Re}(\phi)$ , computed with the higher resolution  $N_{x,col} = N_{y,col} = 40$  and the PML starting at  $x_0 = 2$ .

Using the results at  $l/d=1.8$  as initial values we can vary  $l/d$  and compute the corresponding resonances iteratively via Wielandt iteration. This way we obtain the extended Parker mode diagram depicted in figure 13 for  $0 \leq l/d \leq 4$  and  $0 \leq \text{Re}(f) \leq 2$ . The real parts of the resonances in figures 11 and 12 are reshown as open and filled circles and triangles in figure 13. Also included are the experimental data points of Parker (1966). As far as we know, only results for the trapped Parker modes in the shaded region have been published up to now, see for example Koch (1983) or Evans & Linton (1994).

Analogous resonances are found in cylindrical geometries. For example Linton & McIver (1993) computed the trapped modes in circular cylindrical waveguides with radial fins. Using the above PML approach, we can also compute the corresponding leaky-mode resonances. Arnold, Holste & Rose (2003) demonstrated that these leaky modes are of practical importance in indoor testing of jet engines. There, the leaky-mode resonances are excited by the vortices shed from Pitot tubes in the bellmouth intake of a jet engine during indoor test runs, resulting in high-amplitude discrete noise which is not present in the flight configuration.

In a similar fashion, the resonances can be computed for more complicated structures such as those depicted in figure 9. We demonstrate this for three representative examples. First, we consider the Parker mode problem with the plate

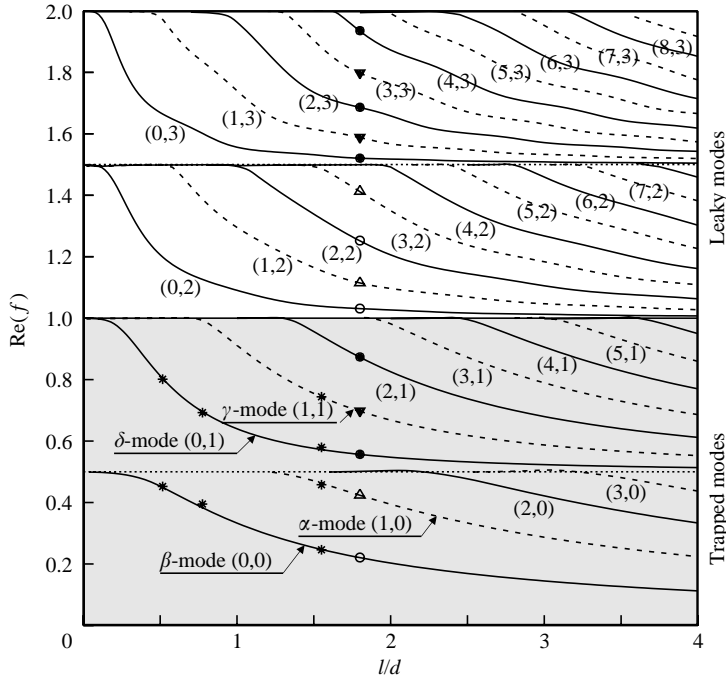


FIGURE 13. Extended Parker mode diagram: resonant frequencies  $\text{Re}(f)$  as function of  $l/d$  computed with  $N_{x,col} = N_{y,col} = 15$ ,  $\sigma_{x,0} = 5$ ,  $d_x = 0.5$ ,  $\beta = 1$ . The stars mark the experimental results for the original  $\alpha$ ,  $\beta$ ,  $\gamma$  and  $\delta$  mode of Parker (1966). The open circles and triangles at  $l/d = 1.8$  are the  $x$ -symmetric and  $x$ -antisymmetric Neumann problem resonances of figure 11. The filled circles and triangles are the  $x$ -symmetric and  $x$ -antisymmetric Dirichlet problem resonances of figure 12.

offset from the centreline of the duct (figure 9c). Evans & Linton (1994) and Evans, Linton & Ursell (1993) published the corresponding trapped mode frequencies for the Neumann problem, and Davies & Parnovski (1998) proved that for an offset plate there always exists at least one trapped mode. For general off-centre structures in a channel with Neumann or Dirichlet boundary conditions on the channel walls, the trapped mode frequencies were examined recently by Linton *et al.* (2002). The transition from a real trapped mode to a complex resonant mode for an arbitrary off-centre obstacle was discussed by Aslanyan, Parnovski & Vassiliev (2000) from a more theoretical point of view. Here we solve the problem numerically by means of the PML method. The off-centre Parker mode problem is no longer symmetric about the  $x$ -axis, but we can still make use of the symmetry and antisymmetry about  $x = 0$ . For  $l/d = 1.8$  and  $c/d = 0.25$  the corresponding resonant frequencies are shown in figure 14. The shaded domain marks the region of trapped modes treated in Evans & Linton (1994), and the first two resonant frequencies correspond to the symmetric and antisymmetric trapped modes of their figure 3 for  $l/d = 1.8$ . The continuous spectra start at the cut-on frequencies  $\text{Re}(f) = 0.5, 1.0, 1.5, \dots$ , i.e. the trapped modes exist only at frequencies below the first cut-on frequency. The pictures at the top of figure 14 show the eigenfunctions  $\text{Re}(\phi)$  of three resonant modes, including the antisymmetric trapped mode corresponding to the mode  $(1, 0)$  in figure 11. We note that, with the exception of the antisymmetric trapped mode, the least damped resonant modes are mostly transversal modes with nodal lines

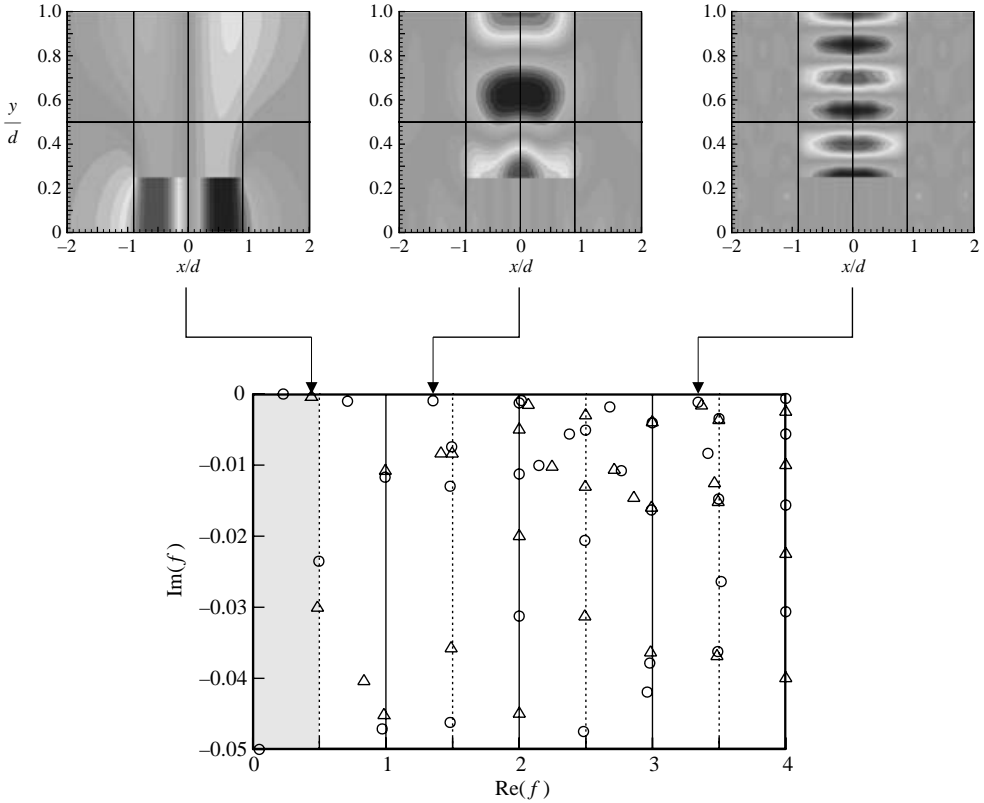


FIGURE 14. Parker mode resonances for the Neumann problem with an offset plate  $l/d = 1.8$ ,  $c/d = 0.25$  corresponding to the example in Evans & Linton (1994).  $N_{x,col} = N_{y,col} = 25$ ,  $\sigma_{x,0} = 5$ ,  $x_0 = 2$ ,  $d_x = 0.5$ ,  $\beta = 1$ .  $\circ$ ,  $x$ -symmetric;  $\triangle$ ,  $x$ -antisymmetric resonances. The top pictures show three examples of resonant eigenfunctions  $\text{Re}(\phi)$ .

parallel to the  $x$ -direction. Similarly, we can compute the resonant frequencies for the Dirichlet problem, extending the trapped mode results of figures 3 and 4 in Linton *et al.* (2002).

Next, we consider a thick plate of thickness  $b$  placed symmetrically in the centre of the channel (figure 9d). The trapped modes for the Neumann problem have been computed by Evans & Linton (1991) for  $0 \leq l/d \leq 6$  and four values of  $b/d$ . For a long rectangle, Khallaf, Parnovski & Vassiliev (2000) provided analytic estimates for the trapped mode frequencies, and the branch structure of the trapped modes was investigated by McIver, Linton & Zhang (2002). Figure 15, computed via the PML method, shows also higher-order resonant modes in addition to the trapped modes for  $l/d = 1.8$  and  $b/d = 0.5$ . The two resonant frequencies in the shaded region correspond to the symmetric and antisymmetric trapped mode of figure 5 in Evans & Linton (1991). The left-hand picture at the top of figure 15 portrays the eigenfunction corresponding to the antisymmetric trapped mode of Evans & Linton (1991). The other two pictures at the top are examples of weakly damped symmetric resonant eigenfunctions. The continuous spectra start at  $\text{Re}(f) = 0.5, 1.5, \dots$ . In this example, the resonant frequencies appear in groups with the same number of nodal lines parallel to the  $x$ -axis and an increasing number of nodal lines parallel to the  $y$ -axis.

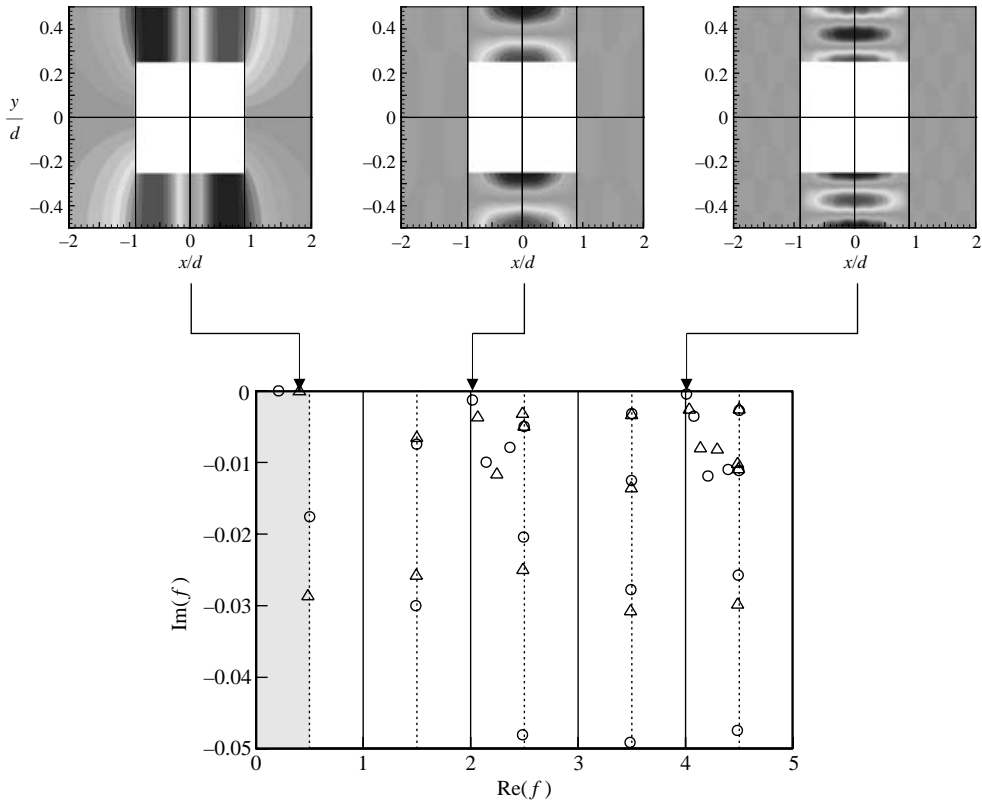


FIGURE 15. Resonances for the Neumann problem of a centred rectangular cylinder with  $l/d=1.8$  and  $b/d=0.5$ .  $N_{x,col}=N_{y,col}=30$ ,  $\sigma_{x,0}=5$ ,  $x_0=2$ ,  $d_x=0.5$ ,  $\beta=1$ .  $\circ$ ,  $x$ -symmetric;  $\triangle$ ,  $x$ -antisymmetric resonances. The top pictures show three examples of resonant eigenfunctions  $\text{Re}(\phi)$ .

A similar computation for the Dirichlet problem does not seem to give any trapped mode, and the resonant modes appear to be highly damped.

Resonances occur also for multi-body structures in a channel. Therefore, as a last example we consider the special case of two plates of zero thickness on the centreline of the channel placed symmetrically about  $x=0$  with a gap in between (figure 9e). Trapped modes with (non-symmetrical) tandem plates in a duct were investigated by Stoneman *et al.* (1988), and are of importance in turbomachines (Woodley & Peake 1999). For cylinders instead of plates along the centreline of the channel, Evans & Porter (1997) showed that in general there are as many trapped modes as there are cylinders. Aligning equally spaced cylinders across the channel, Utsunomiya & Taylor (1999) came to the same conclusion as far as the number of trapped modes is concerned. Porter & Evans (1999) and Linton & McIver (2002) pointed out the close connection of the Neumann and Dirichlet trapped modes in a channel to Rayleigh–Bloch surface waves along infinite periodic structures. Rayleigh–Bloch surface waves propagate along a periodic structure, but decay exponentially away from the structure. In the context of water waves, Rayleigh–Bloch waves correspond to edge waves travelling along a periodic coastline and decaying exponentially out to sea (Evans & Linton 1993; Evans & Fernyhough 1995). Analogous surface waves can be observed also along electromagnetic gratings.

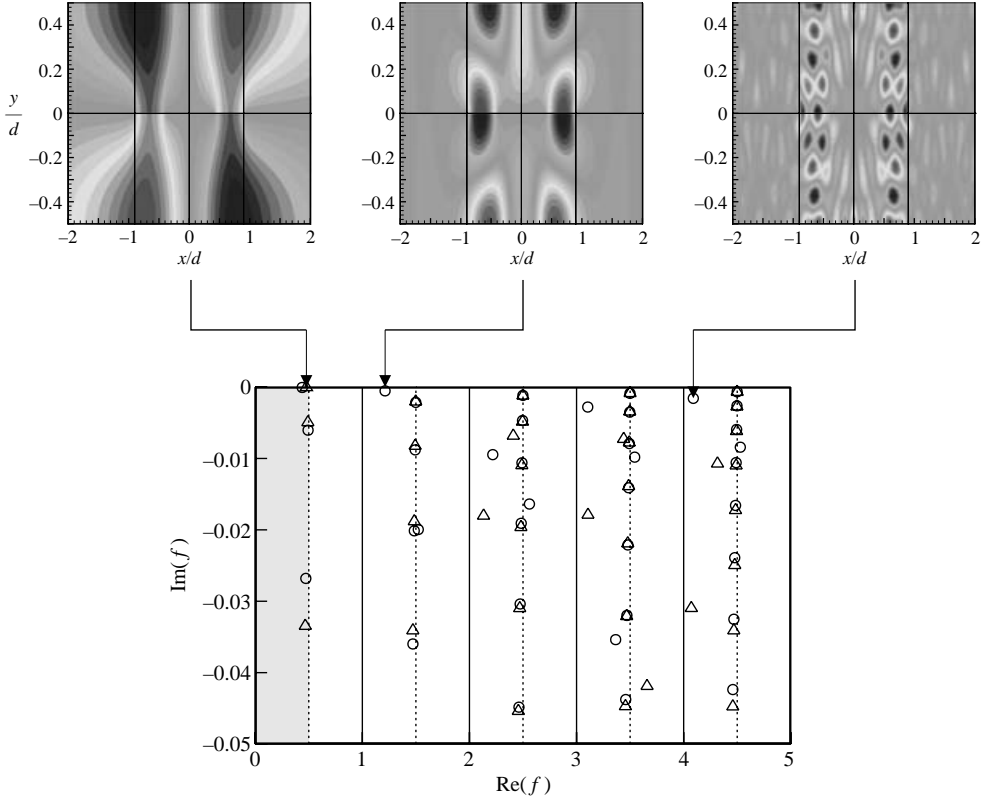


FIGURE 16. Resonances for the Neumann problem of two centred plates of length  $l/d=0.5$  separated by a gap of width  $c/d=0.8$ .  $N_{x,col}=N_{y,col}=30$ ,  $\sigma_{x,0}=5$ ,  $x_0=2$ ,  $d_x=1.0$ ,  $\beta=1$ .  $\circ$ ,  $x$ -symmetric;  $\triangle$ ,  $x$ -antisymmetric resonances. The top pictures show three examples of resonant eigenfunctions  $\text{Re}(\phi)$ .

Returning to our two-plate problem, figure 16 shows the resonant frequencies for the Neumann problem with a plate length  $l/d=0.5$  and a gap  $c/d=0.8$  in between. There are two trapped modes below the first cut-on frequency of the channel. It is of interest to note that, with  $d_x=0.5$ , the antisymmetric trapped mode was slightly unstable, i.e. it had a small positive imaginary part, which is impossible. Increasing the number of collocation points, or doubling the number of domains did not change this. However, when we doubled the PML thickness to  $d_x=1.0$ , the trapped mode frequency was damped and almost real. This shows that the influence of the PML parameters, as outlined in figure 5, is of prime importance for improving numerical results. The three pictures at the top of figure 16 show again the resonant eigenfunctions of three modes, including the antisymmetric trapped mode, corresponding to Parker's  $\alpha$  mode. The symmetrical trapped mode looks similar to the mode shown by Stoneman *et al.* (1988) in their figure 7, and is the one mainly excited in the presence of flow.

In summary, two-dimensional open problems with lateral periodicity still require only a one-dimensional PML, but allow multiple scattering at higher frequencies. As a consequence, several continuous spectra occur which are approximated by the numerical PML solution in addition to the resonances. However, owing to different radiation damping and contrary to closed system resonators, not all resonances are of equal importance. Trapped modes are of special interest, but it should be emphasized

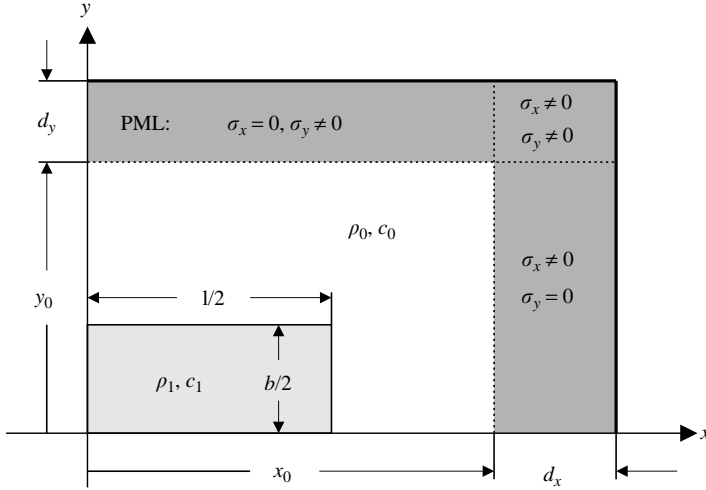


FIGURE 17. Two-dimensional model problem of a rectangular fluid domain with density  $\rho_1^*$  which differs from the density  $\rho_0^*$  in the surrounding fluid. The perfectly matched layers of thickness  $d_x$  and  $d_y$  are located at  $+x_0$  and  $+y_0$ .

that our numerical method cannot distinguish exactly between a genuine trapped mode and a weakly damped leaky mode. At higher frequencies resonant transversal modes with nodal lines parallel to the  $x$ -axis appear to be the least damped.

## 5. Resonances in two-dimensional open systems

### 5.1. Resonances in a rectangular slab with different fluid density

In this final section, the channel walls will be removed and resonances will be computed for completely open two-dimensional structures. For our model problem, this means that we have a rectangular domain of length  $l^*$  and width  $b^*$  containing fluid with different density  $\rho_1^*$  embedded in an infinite fluid with density  $\rho_0^*$ . The speed of sound is assumed to be everywhere  $c_0^*$ , i.e.  $c_1^* = c_0^*$ . In this case  $b^*$ ,  $\rho_0^*$  and  $c_0^*$  are chosen as reference quantities, such that the dimensionless frequency is defined by  $K = \omega^* b^* / c_0^*$  and  $f = K / 2\pi$ .

To eliminate reflected waves in our Cartesian coordinate system, we have to introduce PMLs now in the  $x$ - and  $y$ -directions, as shown by Hu (2004) and outlined in §2. Owing to symmetries, only the quarter-plane problem, sketched in figure 17, needs to be solved with corresponding symmetry and antisymmetry conditions at the  $x$ - and  $y$ -axes. The two-dimensional PML equation, (2.6), has to be applied only in the corner region  $x_0 \leq x \leq (x_0 + d_x)$  and  $y_0 \leq y \leq (y_0 + d_y)$ . In the remaining PML regions, one-dimensional PML equations such as (4.3) suffice. In the following, we show only the  $y$ -symmetric resonant modes with prescribed Neumann condition  $\partial\phi/\partial y = 0$  at  $y = 0$ .

Figure 18 shows the spectrum for  $y$ -symmetric resonances. Again, each resonant mode can be characterized by two integers  $(n, m)$  specifying the number of nodal pressure lines in  $x$ - and  $y$ -directions, respectively. This is analogous to a closed resonator where a Dirichlet or Neumann condition is prescribed at the slab boundary. For open resonators the radiation condition has to be imposed resulting in complex resonant frequencies. We observe that the  $m = \text{const.}$  modes lie along lines starting at

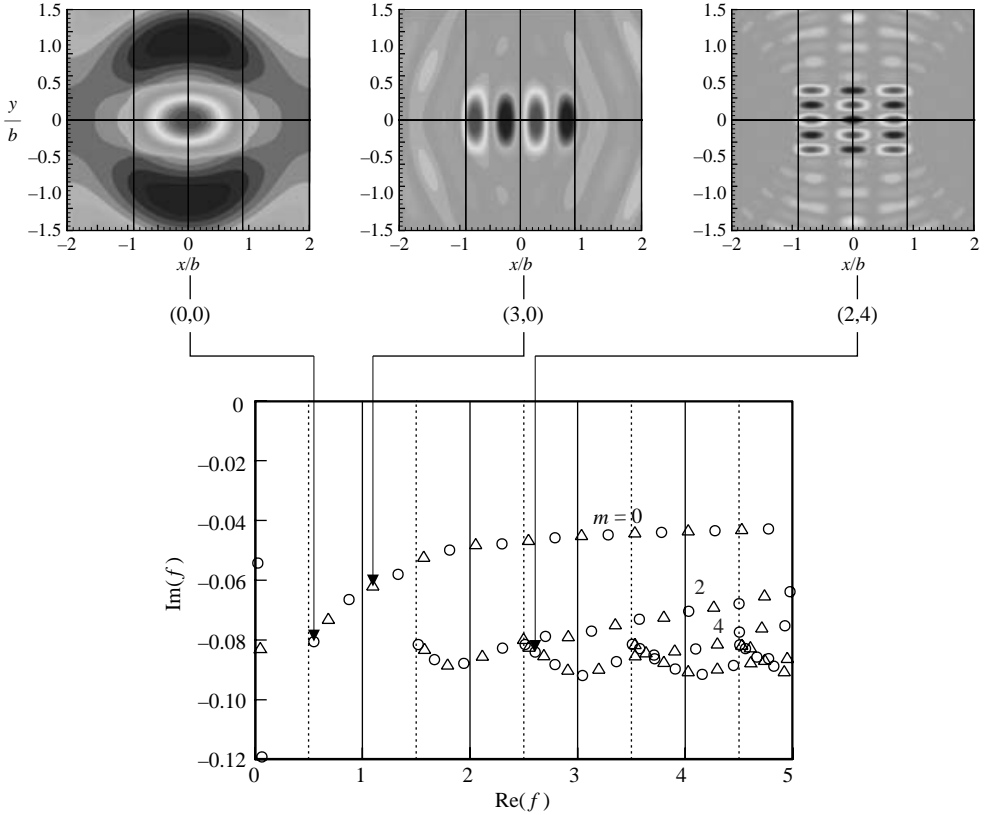


FIGURE 18.  $y$ -Symmetric resonances in a rectangular fluid slab with  $l/b=2$  and  $\rho_1/\rho_0=4$ .  $N_{x,col}=N_{y,col}=30$ ,  $\sigma_{x,0}=\sigma_{y,0}=5$ ,  $x_0=2$ ,  $y_0=1.5$ ,  $d_x=d_y=1.0$ ,  $\beta=1$ .  $\circ$ ,  $x$ -symmetric;  $\triangle$ ,  $x$ -antisymmetric resonances. The top pictures show three examples of resonant eigenfunctions  $\text{Re}(\phi)$ .

the cut-on frequencies, and the imaginary part of the frequency approaches a unique limit as  $n \rightarrow \infty$ , which appears to be close to the one-dimensional result of figure 4. Different from the waveguide problem, depicted in figure 10, here the longitudinal  $m=0$  modes are the least damped. The upper three pictures show the resonant eigenfunctions of the fundamental mode and an  $x$ -antisymmetric and  $x$ -symmetric higher-order mode.

Similarly, the  $y$ -antisymmetric resonances can be computed by imposing a Dirichlet condition along  $y=0$ . The corresponding resonances for the  $m=1, 3, 5, \dots$  modes lie in figure 18 in between the  $y$ -symmetric mode bands  $m=0, 2, 4, \dots$ , but are not shown.

### 5.2. Gap tone resonances

To investigate possible tone generation mechanisms associated with the flow through the gaps of a high-lift system, Tam & Pastouchenko (2001) formulated a generic two-dimensional wall jet model for the slat or flap gap exit. Assuming an infinitely thin trailing edge, they solved the model problem using computational aeroacoustics (CAA) methods. They discovered a feedback mechanism for the transverse gap modes and derived a simple prediction formula for the gap tone frequencies. Agarwal & Morris (2002) extended these ideas by including the sound source characteristics.



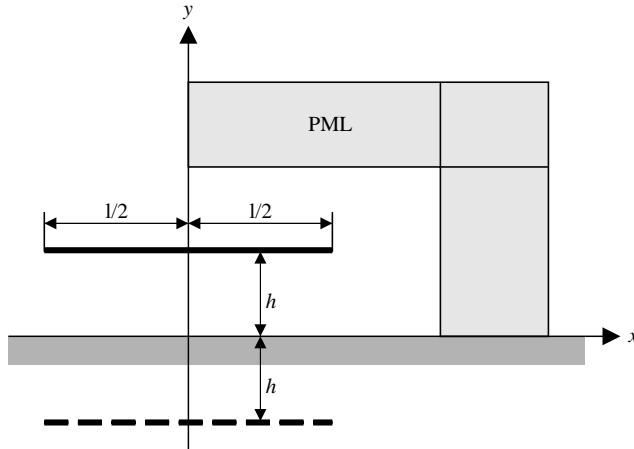


FIGURE 19. Two-dimensional gap tone model for zero mean flow with perfectly matched layers.

For this, they computed the slat wake-shedding frequency as a function of slat trailing-edge bluntness and finite thickness of the slat boundary layers by means of the absolute-convective stability analysis of Koch (1985) and Chomaz, Huerre & Redekopp (1991). If the frequency of the source matches one of the gap's normal modes, a high-amplitude tonal noise would be produced. This is analogous to the mechanism exciting the Parker modes. The transverse gap tone modes obviously constitute only part of the resonances if the plate has finite length. In the present paper, we compute the resonances in such a finite-length problem. While mean flow is important for the sound-generating trailing-edge vortices, it plays only a minor role for the resonances at low Mach numbers, as can be seen from the Parker mode results of Koch (1983). Therefore, in the following, we compute only the resonances of the zero mean flow model depicted in figure 19.

The no-flow gap tone model of figure 19 consists of an infinitely thin sound hard plate of finite length  $l$  located a distance  $h$  above a hard wall. Symmetry or antisymmetry about the  $x = 0$  axis can be assumed for zero mean flow. Adding another mirror image plate below the hard wall and assuming symmetry or antisymmetry also about the  $y = 0$  axis defines a classical two-dimensional laser cavity (Weinstein 1969). Owing to the symmetries, only the quarter-wave problem need be considered. In laser applications, the wavelength is usually much smaller than any characteristic length of the system. For these applications, the approximate methods employed for their computation, such as geometrical optics or the (asymptotic) method of the parabolic equation, are very accurate for the high- $Q$  modes. Contrary to this we are interested in the case where the wavelength is comparable to the characteristic length of the system, and the perfectly matched layer method used in § 5.1 appears well suited for achieving this goal.

Prescribing a Neumann condition  $\partial\phi/\partial y = 0$  for the velocity potential at  $y = 0$ , figure 20 shows our results for  $x$ -symmetric and  $x$ -antisymmetric resonances. For this application we chose the 'cavity' depth  $2h^*$ , i.e. twice the gap height  $h^*$ , as reference length, such that the dimensionless frequency is defined by  $K = \omega^* 2h^* / c_0^*$  and  $f = K / 2\pi$ . The computed frequency spectrum looks very similar to the spectrum sketched in figure 14 of Weinstein (1969), and clearly demonstrates that only a few modes exhibit high  $Q$  factors. It turns out that for zero mean flow, these

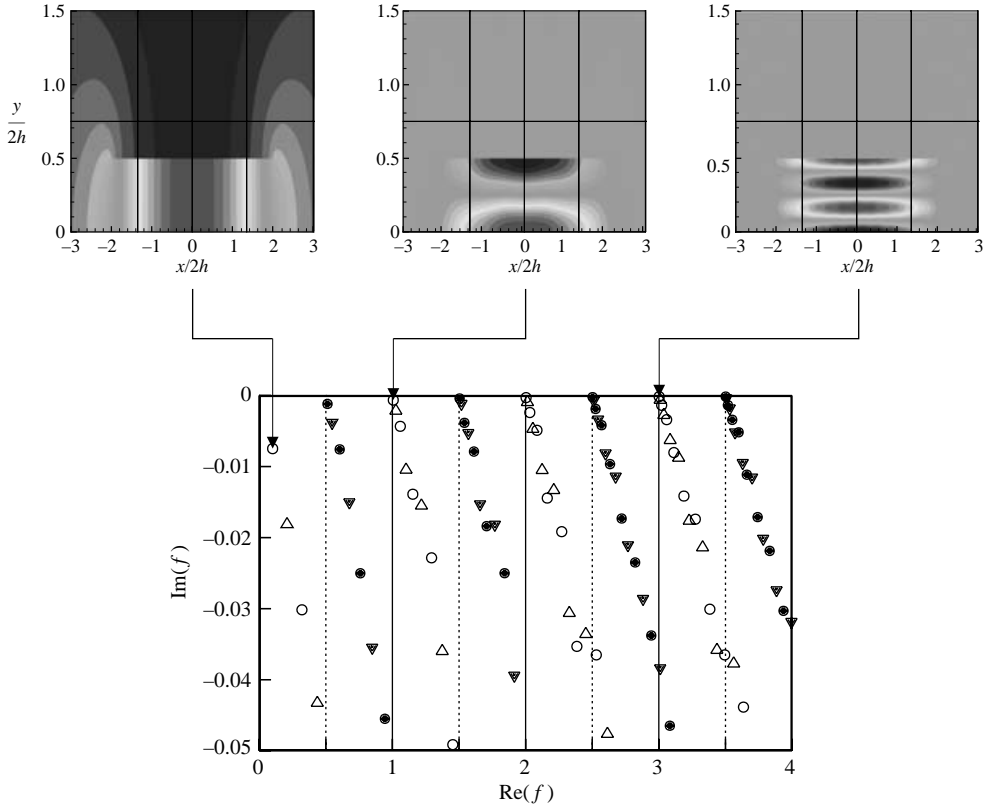


FIGURE 20. Gap tone resonances for  $l/h=8$  with  $N_{x,col}=N_{y,col}=30$ ,  $\sigma_{x,0}=\sigma_{y,0}=5$ ,  $x_0=3$ ,  $y_0=1.5$ ,  $d_x=d_y=1.0$ ,  $\beta=1$ .  $\circ$ ,  $x$ -symmetric;  $\triangle$ ,  $x$ -antisymmetric  $y$ -symmetric gap tone resonances.  $\bullet$ ,  $x$ -symmetric;  $\blacktriangledown$ ,  $x$ -antisymmetric  $y$ -antisymmetric laser mode resonances. The top pictures show three examples of weakly damped resonant gap tone eigenfunctions  $\text{Re}(\phi)$ .

high-Q resonant modes are exactly the transverse gap tone modes of Tam & Pastouchenko (2001). All longitudinal resonant modes have higher radiation losses than the transverse resonant modes. The upper pictures in figure 20 show examples of resonant eigenfunctions, namely the eigenfunctions of the fundamental resonant mode and two transverse resonant modes. The upper right eigenfunction already looks very similar to the pattern of standing waves between two-dimensional plane parallel mirrors shown in figure 9 of Weinstein (1969). The latter figure was drawn from a photograph of Bykov (1964) who used waves on the surface of mercury to model experimentally oscillations in a two-dimensional open resonator. Naturally, for the laser cavity problem, we also have to consider the  $y$ -antisymmetric modes with  $\phi=0$  at  $y=0$ . These  $y$ -antisymmetric resonances start at  $\text{Re}(f)=0.5, 1.5, \dots$  and are shown by the filled symbols in figure 20.

## 6. Conclusion

In the present paper we computed resonances numerically for several open resonators of rectangular geometry by means of a multi-domain spectral collocation method together with PML absorbing boundary conditions. A numerical error analysis, performed for a one-dimensional model problem, which is amenable to

analytic solution, served to demonstrate the influence of the various PML parameters and guided us in choosing these parameters. The obtained results show that the applied complex scaling formulation of the PML method, customary in atomic and molecular physics, is robust and well suited to separate the discrete resonances from the continuous spectrum. In the numerical solution, the latter showed up in discretized form also, but could be discerned easily. A disadvantage of absorbing boundary conditions are the additional computational points in the PML which are physically irrelevant, but are needed to damp the outgoing waves to such a low level that the waves reflected from the outer end of the PML can be neglected. Applying the PML method to a Fabry–Perot cavity, we demonstrated the effect of defects in a one-dimensional bandpass structure.

For open structures in a two-dimensional waveguide, only one-dimensional PMLs are necessary to obtain a solution of the two-dimensional Helmholtz equation satisfying the radiation condition. For each cut-on duct mode, a continuous spectrum appears; but, in general, the resonances can be separated quite well from these continuous spectra. We reconsidered the Parker mode problem and were able to compute, in our opinion for the first time, leaky Parker modes in addition to the classical trapped Parker modes. In applications, such leaky modes are often more important than trapped modes, cf. the water wave example of Maniar & Newman (1997). Several generalizations of the Parker mode problem were treated, such as an offset plate, a thick plate, or tandem plates. In all these problems, only few resonances are weakly damped and therefore have a high  $Q$  factor. We observed that most of these weakly damped resonances are transversal resonant modes.

Finally, we considered resonances in completely open two-dimensional structures. For our rectangular domains, PMLs had to be applied in both coordinate directions. Of particular interest was the gap noise model problem of Tam & Pastouchenko (2001). It turned out that for zero mean flow, the high- $Q$  resonant modes are exactly the transverse gap tone modes of Tam & Pastouchenko (2001). In general, we can state that, contrary to resonances in closed systems, only few resonances are weakly damped in open systems and hence are of physical relevance. This is well known in the design of laser cavities, (Weinstein 1969). Therefore, it will be of great interest to compute the resonances for a realistic slat geometry of a high lift configuration and determine the resonances of importance. If these resonances are near any self-excited shear-layer frequency one can expect high noise levels and enhanced airframe noise in analogy to the Parker mode problem.

The PML method can easily be generalized to compute resonances in open three-dimensional structures, see for example Hu (2004). However, the corresponding eigenvalue problems are in general extremely large. Therefore, exploring the full spectrum with adequate resolution is not feasible at present and we have to make use of Krylov subspace methods in order to obtain the resonances in a particular frequency domain. The resonant field around the open structure can then be used to compute the far-field pattern of that resonant mode with the help of Green's representation formula (Colton & Kress 1997, theorem 2.4), as done, for example, in Hwang *et al.* (1998) for a related electrodynamic problem (note that they used  $e^{+i\omega t}$  instead of  $e^{-i\omega t}$ ).

We would like to dedicate this paper to the memory of Ralph Parker who pioneered the idea of acoustic resonances in turbomachinery cascades and ducts containing plates. We are grateful to Jay Hardin and two referees for constructive criticism. Part of this work was funded by the German Aerospace Research Programme.

## REFERENCES

- AGARWAL, A. & MORRIS, P. 2002 Investigation of the physical mechanisms of tonal sound generation by slats. *AIAA Paper* 2002-2575.
- AGUILAR, J. & COMBES, J. 1971 A class of analytic perturbations for one-body Schrödinger Hamiltonians. *Commun. Math. Phys.* **22**, 269–279.
- ARNOLD, F., HOLSTE, F. & ROSE, M. 2003 The whistling pitot probe – an example for aeroacoustic feedback mechanism in a practical application. Paper presented at DGLR-Fachausschuss-Sitzung T2.3 ‘Strömungsakustik/Fluglärm’ at the TU Dresden, 10 January 2003.
- ASLANYAN, A., PARNOVSKI, L. & VASSILIEV, D. 2000 Complex resonances in acoustic waveguides. *Q. J. Mech. Appl. Maths* **53**, 429–447.
- BASLEV, E. & COMBES, J. 1971 Spectral properties of many body Schrödinger operators with dilation analytic interactions. *Commun. Math. Phys.* **22**, 280–294.
- BÉRENGER, J. 1994 A perfectly matched layer for the absorption of electromagnetic waves. *J. Comput. Phys.* **114**, 185–200.
- BREKHOVSKIKH, L. 1960 *Waves in Layered Media*. Academic.
- BYKOV, V. 1964 In *High Power Electronics*, vol. 3, pp. 148–153. Nauka, Moscow.
- CALLAN, M., LINTON, C. & EVANS, D. 1991 Trapped modes in two-dimensional waveguides. *J. Fluid Mech.* **229**, 51–64.
- CANUTO, C., HUSSAINI, M., QUARTERONI, A. & ZANG, T. 1988 *Spectral Methods in Fluid Dynamics*. Springer.
- CHEW, W., JIN, J. & MICHIELSEN, E. 1997 Complex coordinate stretching as a generalized absorbing boundary condition. *Microwave Optical Technol. Lett.* **15**, 144–147.
- CHEW, W. & WEEDON, W. 1994 A 3-D perfectly matched medium from modified Maxwell’s equation with stretched coordinates. *Microwave Optical Technol. Lett.* **7**, 599–604.
- CHOMAZ, J.-M., HUERRE, P. & REDEKOPP, L. 1991 A frequency selection criterion in spatially developing flows. *Stud. Appl. Maths* **84**, 119–114.
- COLTON, D. & KRESS, R. 1997 *Inverse Acoustic and Electromagnetic Scattering Theory*, 2nd edn. Springer.
- COOPER, A. & PEAKE, N. 2000 Trapped acoustic modes in aeroengine intakes with swirling flow. *J. Fluid Mech.* **419**, 151–175.
- DAVIES, E. & PARNOVSKI, L. 1998 Trapped modes in acoustic waveguides. *Q. J. Mech. Appl. Maths* **51**, 477–492.
- DOBRYNSKI, W., GEHLHAR, B. & BUCHHOLZ, H. 2001 Model and full scale high-lift wing wind tunnel experiments dedicated to airframe noise reduction. *Aerosp. Sci. Technol.* **5**, 27–33.
- ELEJABARRIETTA, M., SANTAMARIA, C. & EZCURRA, A. 2002 Air cavity modes in the resonance box of the guitar: the effect of the sound hole. *J. Sound Vib.* **252**, 584–590.
- EVANS, D. & FERNYHOUGH, M. 1995 Edge waves along periodic coastlines. Part 2. *J. Fluid Mech.* **297**, 307–325.
- EVANS, D., LEVITIN, M. & VASSILIEV, D. 1994 Existence theorems for trapped modes. *J. Fluid Mech.* **261**, 21–31.
- EVANS, D. & LINTON, C. 1991 Trapped modes in open channels. *J. Fluid Mech.* **225**, 153–175.
- EVANS, D. & LINTON, C. 1993 Edge waves along periodic coastlines. *Q. J. Mech. Appl. Maths* **46**, 644–656.
- EVANS, D. & LINTON, C. 1994 Acoustic resonance in ducts. *J. Sound Vib.* **173**, 85–94.
- EVANS, D., LINTON, C. & URSELL, F. 1993 Trapped mode frequencies embedded in the continuous spectrum. *Q. J. Mech. Appl. Maths* **46**, 253–274.
- EVANS, D. & PORTER, R. 1997 Trapped modes about multiple cylinders in a channel. *J. Fluid Mech.* **339**, 331–356.
- EXNER, P., ŠEBA, P., TATER, M. & VANĚK, D. 1996 Bound states and scattering in quantum waveguides coupled laterally through a boundary window. *J. Math. Phys.* **37**, 4867–4887.
- FOWLES, G. 1968 *Introduction to Modern Optics*. Holt, Rinehart and Winston.
- FRANKLIN, R. 1972 Acoustic resonance in cascades. *J. Sound Vib.* **25**, 587–595.
- GIVOLI, D. 1999 Recent advances in the DtN FE method. *Arch. Comput. Meth. Engng* **6**, 71–116.
- GROSCHKE, F.-R., SCHNEIDER, G. & STIEWITT, H. 1997 Wind tunnel experiments on airframe noise sources of transport aircraft. *AIAA Paper* 97-1642.

- HASTINGS, F., SCHNEIDER, J. & BROCHAT, S. 1996 Application of the perfectly matched layer (PML) absorbing boundary condition to elastic wave propagation. *J. Acoust. Soc. Am.* **100**, 3061–3069.
- HILE, C. & KRIEGSMANN, G. 1998 A hybrid numerical method for loaded highly resonant single mode cavities. *J. Comput. Phys.* **142**, 506–520.
- HISLOP, P. & SIGAL, I. 1996 *Introduction to Spectral Theory*. Springer.
- HU, F. 1996 On absorbing boundary conditions for linearized Euler equations by a perfectly matched layer. *J. Comput. Phys.* **129**, 201–219.
- HU, F. 2001 A stable perfectly matched layer for linearized Euler equations in unsplit physical variables. *J. Comput. Phys.* **173**, 455–480.
- HU, F. 2002 On constructing stable perfectly matched layers as an absorbing boundary condition for Euler equations. *AIAA Paper* 2002-0227.
- HU, F. 2004 Absorbing boundary conditions. *Intl J. Comput. Fluid Dyn.* (to appear).
- HUTCHINS, C. 1962 The physics of violins. *Sci. Am.* **207**, 78–93.
- HWANG, J.-K., HYUN, S.-B., RYU, H. & LEE, Y.-H. 1998 Resonant modes of two-dimensional photonic bandgap cavities determined by the finite-element method and by use of the anisotropic perfectly matched layer boundary condition. *J. Opt. Soc. Am. B* **15**, 2316–2324.
- HYUN, S., HWANG, J., LEE, Y. & KIM, S. 1997 Computation of resonant modes of open resonators using the FEM and the anisotropic perfectly matched layer boundary condition. *Microwave Opt. Technol. Lett.* **16**, 352–356.
- IHLENBURG, F. 1998 *Finite Element Analysis of Acoustic Scattering*. Springer.
- KARLSSON, H. 1998 Accurate resonances and effective absorption of flux using smooth exterior scaling. *J. Chem. Phys.* **109**, 9366–9371.
- KHALLAF, N., PARNOVSKI, L. & VASSILIEV, D. 2000 Trapped modes in a waveguide with a long obstacle. *J. Fluid Mech.* **403**, 251–261.
- KHORRAMI, M., BERKMAN, M. & CHOUDHARI, M. 2000 Unsteady flow computations of a slat with a blunt trailing edge. *AIAA J.* **38**, 2050–2058.
- KOCH, W. 1983 Resonant acoustic frequencies of flat plate cascades. *J. Sound Vib.* **88**, 233–242.
- KOCH, W. 1985 Local instability characteristics and frequency determination of self-excited wake flows. *J. Sound Vib.* **99**, 53–83.
- KOKKOTAS, K. & SCHMIDT, B. 1999 Quasi-normal modes of stars and black holes. *Living Rev. Rel.* **2**, 2–95.
- KRIEGSMANN, G. 2003 Scattering matrix analysis of a photonic Fabry–Perot resonator. *Wave Motion* **37**, 43–61.
- LINTON, C. & McIVER, M. 2002 The existence of Rayleigh–Bloch surface waves. *J. Fluid Mech.* **470**, 85–90.
- LINTON, C., McIVER, M., McIVER, P., RATCLIFFE, K. & ZHANG, J. 2002 Trapped modes for off-centre structures in guides. *Wave Motion* **36**, 67–85.
- LINTON, C. & McIVER, P. 1993 Acoustic resonances in the presence of radial fins in circular cylindrical waveguides. *Wave Motion* **18**, 51–65.
- MANIAR, H. & NEWMAN, J. 1997 Wave diffraction by a long array of cylinders. *J. Fluid Mech.* **339**, 309–330.
- McIVER, M., LINTON, C. & ZHANG, J. 2002 Branch structure of embedded trapped modes in two-dimensional waveguides. *Q. J. Mech. Appl. Maths* **55**, 313–326.
- MEYER, E. & POTTEL, R. 1969 *Physikalische Grundlagen der Hochfrequenztechnik*. Vihweg & Sohn.
- MOISEYEV, N. 1998 Quantum theory of resonances: calculating energies, widths and cross-sections by complex scaling. *Phys. Rep.* **302**, 211–293.
- NAYFEH, A. & HUDDLESTON, D. 1979 Resonant acoustic frequencies of parallel plates. *AIAA Paper* 79-1522.
- OLSON, S. 2003 Slat tonal noise mechanisms in a two-dimensional multi-element airfoil configuration. PhD thesis, Notre Dame University.
- PARKER, R. 1966 Resonance effects in wake shedding from parallel plates: some experimental observations. *J. Sound Vib.* **4**, 62–72.
- PARKER, R. 1967 Resonance effects in wake shedding from parallel plates: calculation of resonant frequencies. *J. Sound Vib.* **5**, 330–343.
- PARKER, R. & STONEMAN, S. 1989 The excitation and consequences of acoustic resonances in enclosed fluid flow around solid bodies. *Proc. Instn Mech. Engrs* **203**, 9–19.

- PIERCE, A. 1981 *Acoustics*. McGraw-Hill.
- PORTER, R. & EVANS, D. 1999 Rayleigh–Bloch surface waves along periodic gratings and their connection with trapped modes in waveguides. *J. Fluid Mech.* **386**, 233–258.
- QI, Q. & GEERS, T. 1998 Evaluation of the perfectly matched layer for computational acoustics. *J. Comput. Phys.* **139**, 166–183.
- SACKS, Z., KINGSLAND, D., LEE, R. & LEE, J. 1995 A perfectly matched anisotropic absorber for use as an absorbing boundary condition. *IEE Trans. Antennas Propagat.* **43**, 1460–1463.
- SCHRÖDER, C. & SCOTT, JR, W. 2000 A finite-difference model to study the elastic-wave interactions with buried land mines. *IEEE Trans. Geosci. Remote Sensing* **38**, 1505–1512.
- SIMON, B. 1973 The theory of resonances for dilation analytic potentials and the foundations of time dependent perturbation theory. *Ann. Math.* **97**, 247–274.
- STONEMAN, S., HOURIGAN, K., STOKES, A. & WELSH, M. 1988 Resonant sound caused by flow past two plates in tandem in a duct. *J. Fluid Mech.* **192**, 455–484.
- TAM, C. 1998 Advances in numerical boundary conditions for computational aeroacoustics. *J. Comput. Acoustics* **6**, 377–402.
- TAM, C., AURIAULT, L. & CAMBULI, F. 1998 Perfectly matched layer as an absorbing boundary condition for the linearized Euler equations in open and ducted domains. *J. Comput. Phys.* **144**, 213–234.
- TAM, C. & PASTOUCHENKO, N. 2001 Gap tones. *AIAA J.* **39**, 1442–1448.
- TSYMKOV, S. 1998 Numerical solution of problems on unbounded domains. A review. *Appl. Num. Maths* **27**, 465–532.
- TURKEL, E. & YEFET, A. 1998 Absorbing PML boundary layers for wave-like equations. *Appl. Num. Maths* **27**, 533–557.
- URSELL, F. 1987 Mathematical aspects of trapping modes in the theory of surface waves. *J. Fluid Mech.* **183**, 421–437.
- UTSUNOMIYA, T. & TAYLOR, R. 1999 Trapped modes around a row of circular cylinders in a channel. *J. Fluid Mech.* **386**, 259–279.
- VAHDATI, M., SAYMA, A., BRÉARD, C. & IMREGUN, M. 2002 Computational study of intake duct effects of fan flutter stability. *AIAA J.* **40**, 408–418.
- VENAKIDES, S., HAIDER, M. & PAPANICOLAOU, V. 2000 Boundary integral calculation of two-dimensional electromagnetic scattering by photonic crystal Fabry–Perot structures. *SIAM J. Appl. Maths* **60**, 1686–1706.
- WEINSTEIN, L. 1969 *Open Resonators and Open Waveguides*. Golem, Boulder, Colorado.
- WOODLEY, B. & PEAKE, N. 1999 Resonant acoustic frequencies of a tandem cascade. Part 1. Zero relative motion. *J. Fluid Mech.* **393**, 215–240.
- ZURMÜHL, R. 1961 *Matrizen und ihre technischen Anwendungen*, 3rd edn. Springer.